JUAN GABRIEL CORREA PÉREZ

Laboratório de Dinâmica e Modelagem Oceânica -DinaMO

Regional turbulence patterns driven by meso- and submesoscale processes in the Caribbean Sea

FURG

Rio Grande
2016

JUAN GABRIEL CORREA PÉREZ

Laboratório de Dinâmica e Modelagem Oceânica -DinaMO

Regional turbulence patterns driven by meso- and submesoscale processes in the Caribbean Sea

Dissertação apresentada ao Instituto de Oceanografía da Universidade Federal do Rio Grande (FURG), para a obtenção de Título de Mestre em Oceanografía Física, Química e Geológica.

Orientador: Paulo H. R. Calil

Rio Grande
2016

Juan Gabriel Correa Pérez
    Regional turbulence patterns driven by meso- and sub-mesoscale processes in the Caribbean Sea
    64 páginas
    Dissertação (Mestrado)
Instituto de Oceanografía
Universidade Federal do Rio Grande (FURG).

1. Mesoscale Dynamics

2. Submesoscale Dynamics

3. Caribbean Sea Circulation

4. Model and configurations ROMS

5. Frontogenesis on Mixed Layer

6. Turbulence and KE Spectal Analysis

7. KE decomposition

8. KE spatial Transference

Dissertation Committee:

Prof. Dr. **Paulo H. R. Calil**
Chairperson

Prof. Dr. **Xavier Capet**
Extrenal Judge

Prof. Dr. **José Luis Azevedo Lima**
Internal Judge

Dedico esta tesis a mis padres, Elnidia y Hernan, quienes siempre me brindaron lo mejor de sus vidas: su amor, su valores y nuestra familia
También dedico también este trabajo a mi abuelo Graciano, y a mi abuela Maria Luisa que ahora me acompaña desde el cielo

Acknowledgements

I want to express my sincerally grateful to my advisor Paulo H. R. Calil, by his collaboration, teachings of ocean dynamics and for allowing me to pursue my own research interests.

Thanks are due to all members of DinaMo "Never Abandon", for the collaboration and for allowing me the space for disscution and understanding of the fascinating world of oceanography.

I would also like to extend my sincere gratitude to another professors of the FURG, specially to José Luiz Lima de Azevedo, for the availability and didactic lessons during my formation proccess as master. To Xavier Caper, for participating in my committee and providing suggestions throughout these last time of research.

I would also like to acknowledge Osmar O. Möller, Alberto Piola and Raul Guerrero , for allow me participate in the survey oceanographic SAMOC X in the year 2014. It was a rewarding experience that confirms me that I made the right decision with the change my profesional carreer.

Infinite thanks are due to Mara K. P. Zuleta, for be my lifemate in all this time away from home, she never leaves me feel alone and changes difficult times for wonderful times.

Thanks are also due to my life friends Daniel y Camilo, to my undergraduate professors and another persons that either way ever supported me.

Finall, I would like to thanks my parents, my brother, my grandfather and all my family. I had them in my mind ever, despite of the distance.

Resumo

Neste estudo usamos uma modelagem regional com diferentes resoluções espaciais ($6km$ e $3km$), focando na ressurgência da Guajira e nas Antilhas Menores, no mar do Caribe. A dinâmica superficial nesta região varia desde correntes de larga escala até filamentos costeiros das ressurgências. A interação dos anéis da Corrente Norte do Brasil com as Antilhas pode levar à formação de filamentos de vorticidade na submesoescala no lado protegido das ilhas, transferindo energia cinética (KE) das maiores escalas para as menores, permitindo a advecção de vorticidade potencial (PV). O Sistema de Ressurgências do Caribe (CUS) nas costas da Venezuela e da Colômbia interage com o escoamento da mesoescala, permitindo a formação de filamentos de submesoescala, vórtices menores e a troca vertical de propriedades físicas, que podem fornecer KE para as escalas maiores. Velocidades ageostróficas e velocidades verticais maiores são evidentes nos escoamentos com número de Rossby da ordem O(1), reduzindo a inclinação do espectro de KE nos números de onda (k) maiores e aumentando a divergência do fluxo de traçadores, que demostram a importância dos processos de frontogênesis na camada de mistura das áreas de estudo. Finalmente, o balanço de KE mostra a dominância dos termos dissipativos próximo às ilhas e um aporte de KE sobre a região da ressurgência da Guajira. Isto demostra que os processos de submesoescala no mar do Caribe podem ser potencialmente importantes na dinâmica de larga escala na região.

Keywords: Mar do Caribe, submesoescala, Energia Cinética, Analise Espectral

Abstract

In this study we use a regional model with different spatial resolutions ($6km$ and $3km$), focusing the Guajira Upwelling and the Lesser Antilles in the Caribbean Sea. The upper ocean dynamics in this region ranges from large-scale currents to coastal upwelling filaments. The interaction of North Brazil Current rings with the Antilles may lead to the formation of submesoscale vorticity filaments leeward of the islands, transferring kinetic energy (KE) from large to small scales and allowing the advection of potential vorticity (PV). The Caribbean Upwelling System (CUS) in the coasts of Venezuela and Colombia interacts with the mesoscale flow allowing the formation of submesoscale filaments, small eddies and the vertical exchange of physical properties that may supply KE to larger scales. The ageostrophic velocities and large vertical velocities are evidenced by O(1) Rossby number, the shoaling of the KE spectra in large wavenumbers (k) and affect the eddy flux divergence of tracers which demonstrate the importance of processes such as surface frontogenesis on the mixed layer of the areas of study. Finally, the KE budget exhibits the dominance of dissipative terms near the islands and an injection of KE over the Guajira Upwelling Region. This demonstrates that submesoscale processes in the Caribbean Sea could be potentially important in the large-scale dynamics in the region.

Keywords: Caribbean Sea, submesoscale, Kinetic Energy, Spectral Analyses

Contents

Acrônimos

ASC	Ageostrophic Secondary Circulation
$AVHRR$	Advance Very High Resolution Radiometer
BC	Baroclínico
BT	Barotrópico
BTS	Baroclinic Time Scale
CCS	California Current System
$CLLJ$	Caribbean Low Level Jet
CUS	Caribbean Upwelling System
CCU	Caribbean Coastal Undercurrent
$COADS$	Comprehensive Ocean-Atmosphere Data Set
EKE	Eddie Kinetic Energy
fft	Fast Fourier Transform
$ITCZ$	Inter Tropical Convergence Zone
k	Wavenumber
KE	Kinetic Energy
$NBCr$	North Braziliam Current rings
NEC	North Equatorial Current
$NOAA - NGDC$	NOAA National Geophysical Data Center
PE	Potential Energy
PV	Potential Vorticity
R	Rossby Number
$R_D - L_D$	Rossby Deformation Radio
sCC	Southern Caribbean Current
$SODA$	Simple Ocean Data Assimilation
SST	Sea Surface Temperature
SSH	Sea Surface Heigh

List of Figures

List of Tables

Chapter 1

Introduction

1.1 Mesoscale Circulation

The large and mesoscale circulation is assumed as horizontal motion in the mixed layer, since the horizontal velocities are significantly more higher than the vertical velocities, this hinders the interaction with the layer under the pycnocline. The effect of rotation of the Earth makes that the flow of large-scale in the ocean is accelerated, intensifying the western currents and slowing the eastern currents of the subtropical gyres. This, together to the wind effects generate instabilities that allow the vertical flux between mixed layer and pycnocline, altering the geostrophic balance and enhancing the turbulent motion in the surface layer. This makes that the large and mesoscale motion are consider as the main transport or flux of heat and passive properties between the Equator and poles and have relevant importance in the climate regulation in the Earth.

The mesoscale circulation is considered like one of more energetic motion in the geophysical fluids, this motion is dominated basically by the geostrophy balance between the Coriolis force and hydrostatic pressure in the momentum budget. Its main forcing mechanisms are instabilities from the large-scale circulation such as interactions between currents, conservation of the potential vorticity and the direct forcing of the wind. The

mains structures fixed in the mesoscale range are currents, retroflections, eddies, fronts and upwelling systems. All these structures are sized from ten to several hundred of kilometers in the spacial scales and from weeks to seasonal time scales.

1.2 Frontal and Submesoscale Circulation

As the mesoscale is originate by the instabilities in the large-scale, the submesoscale also results from instabilities of mesoscale circulation. Submesoscale are common in the regions with large lateral density gradient, such as the filaments or fronts of eddies. This destabilized the balance of thermal wind, increasing the vertical turbulence by vertical shear of horizontal velocities while the front is being stirred. Thereby, the secondary ageostrophic circulation appears by the breakdown of the geostrophic balance and vertical velocities are intensified, comparing with the vertical velocities associated with the mesoscale. Due to these ageostrophic velocities are large, the Rossby number increase and Richardson number decreases until values closed to one (R_o and R_i $O(1)$), so we can have the follow relation:

$$R_o = \frac{\zeta}{f} = \frac{U}{fL} \approx 1$$

$$R_i = \frac{N^2 H^2}{U^2}$$

$$F_R = \frac{1}{\sqrt{R_i}} = \frac{U}{NH}$$

Where U is the order magnitude's velocity $O(10^{-1})$, f is the Coriolis parameter $O(10^{-5})$, L is the length scale and H is the mixed layer depth $O(10^1)$. If we make a balance between the Froude Number (F_R) and the Rossby Number R_o , we get de Burger Number B_r that under the considerations been assumed above, B_r is the $O(1)$ too, so

we can get the horizontal scale as follow:

$$\frac{F_r}{R_o} = \frac{fL}{NH} \approx 1 \rightarrow L = \frac{NH}{f}$$

where L is the horizontal scale of submesoscale, making a scale analyse we get:

$$L = \frac{O(10^{-3})O(10^1)}{O(10^{-5})} = O(10^3) = 1km$$

Thus, we can define that length scale of submesoscale around of $O(1km)$ for mid-latitudes where the mixed layer is shallower, as the mixed layer deepen in the tropical latitues the submesoscale range can be one level of magnitud bigger too, while the temporal scale is $O(1day)$.

Submesoscale instabilities are important for exchange of properties in the mixed layer base, it favours the entrainment/detrainment of water masses and nutrients below the pycnocline (Boccaletti et al., 2007), the same manner can induces potential vorticity to and from the surface to interior ocean and the change in stratification of the mixed layer (Thomas et al., 2008).

1.3 Transference of Energy

The transference of energy among oceanic scales depend strongly of turbulence in stratified fluids. Where the conversion between Potential and Kinetic Energy (PE and KE hereinafter) allows to restratify or destratify the mixed layer (Cushman-Roisin and Beckers, 2011). Thereby, it transfers the energy in direct cascade is associated from the large to the smaller scales, while the inverse cascade from the smaller to larger, depending of dominants terms in the events that happen between different scales. This allows establish a two-dimensional turbulence that can develop inverse KE cascade from scales closed to Rossby first baroclinic deformation radius L_D to

larger scales. Another three-dimensional turbulence in which the isotropic flow transfer the KE toward cascade in the smaller scales (Vallis (2006), Scott and Wang (2005)). This latter author summarized and proposed a spectral kinetic energy flux $\pi(k)$ as the flux of KE through the wavenumber k (wavelength λ) as shown Fig. 1.1) based in the geostrophic turbulence theory. They suggest that direct cascade is dominated by baroclinic (BC) mode, while the barotropic (BT) mode works for inverse cascade. This coincide with the Boccaletti et al. (2007) suggestions, over the dominance of the mesoscale regime in the stirring and mixing of the boundary layer and growth in the eddy size. Whereas the submesoscale regime restratifies the mixed layer, enhances the vertical velocities and makes more isotropic the flow, therefore it serves as inertial range between the larger and smaller scales.
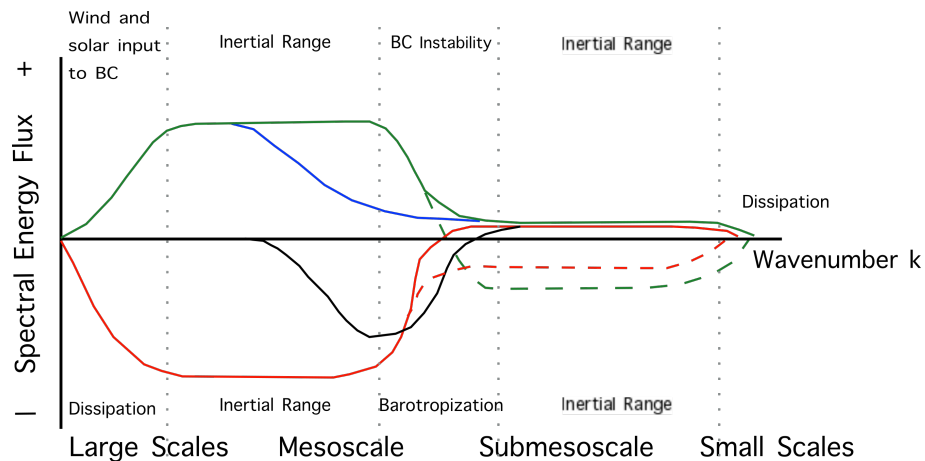
Figure 1.1: (Schematic of spectral total energy flux $\pi(k)$ for the baroclinic mode (green line) and barotropic mode (red line). For the baroclinic mode, the total energy includes a potential energy component. The solid lines are interpreted in terms of spectral flux from Salmon's (1980) and the dashed lines are the modifications to the spectral flux implicit in Rhines's (1977). The blue line was a propose modification of Scott and Wang (2005) to the baroclinic total energy cascade, which is reduced in amplitude by an upscale flux of kinetic energy shown in black. The black line is assumed to be of similar shape to the universal kinetic energy flux found in the altimeter data. Moving upscale, this baroclinic flux peters out, he suspected, because of barotropization. Scheme is extracted from Scott and Wang (2005))

In the Figure 1.1, positive values of $\pi(k)$ mean transfer KE forward cascade and

negative values inverse cascade. Thus, notice as BC mode (green line) and BT mode (red line) tends to transfer energy to direct cascade in scales lesser than the L_D for the first BC mode. While for the dashed line, that was calculating with several BC modes, both modes can transfer for higher scales in the closed range of L_D and submesoscale range. Scott and Wang (2005) proposed that in vicinity scales of L_D can happen the barotropization process where can reverts the cascade flow, providing EK from mesoscale for large-scales, while the submesoscale range remains like inertial range in the EK flux $\pi(k)$ forward cascade for both modes.

1.4 Structure of the Dissertation

The present study will focus on the turbulent motion in the region of the Caribbean Sea, emphasizing in the areas around the Lesser Antilles and the Guajira Peninsula, with special attention given to submesoscale dynamic and processes of energy transference.

This work is organized as follows. In Chapter 2, we describe the main mesoscale circulation inside and surroundings of Caribbean Sea, emphasizing in the locations and processes where we believe can develop a submesoscale dynamic. In chapter also shows the configurations and validation of Regional Ocean Modeling System (ROMS) that now is knows as Coastal and Regional Ocean Community Model (CROCO), it was apply to reproduce the ocean dynamics with high resolution in our region of study.

In Chapter 3, the Manuscript explains how the mesoscale circulation can interacts with the submesoscale dynamic and enhance the exchange of physical properties between the mixed layer and the interior ocean, understanding the energy transference between the two scales in the Caribbean Sea.

The Chapter 4 contains a summary of the results, final considerations and some ideas for future research are given

Chapter 2

Theoretical Background

2.1 Description of Study Area

Due to its nearness to Equator, the Caribbean Sea receives most radiation along of whole year and it is reflected in its higher sea surface temperature (SST), the deepen the pycnocline and increasing of the mixed layer, for this reason is named as Atlantic Warm Pool where the SST mean is upper of $28°C$. SST field has a seasonal variation by the meridional migration of Inter-Tropical Convergence Zone (Wang et al., 2006). The wind stress curl and Ekman transport in the Guajira Peninsula (Colombia) and Margarita Island (Venezuela) originate the Caribbean Upwelling System (CUS), where some filaments of cool water and chlorophyll are pulled offshore and contrast with the homogeneous and warmer water in the center of the basin (Andrade and Barton (2005), Rueda-Roa and Muller-Karger (2013)).

The large and mesoscale motion of the Caribbean Sea and its surroundings present one of more dynamic variability in the oceanic and atmospheric circulation in the whole world, because it is influenced by the combined effect of several oceanic process that we summarized next and was schematize in the Fig. 17 of Jouanno et al. (2008):

- The North Equatorial Current (NEC)(Johns et al., 2002) interacts with the island

chain of the Lesser Antilles and continue within the Caribbean with the name of South Caribbean Current (sCC).

- The North Brazil Current occasionally retroflects and shed large isolated warm-core rings (NBCr) exceeding 450 km in overall diameter. This rings dislocates north-westward until the vicinities of Lesser Antilles, where are decomposed (Fratantoni and Richardson, 2006) and can transferring instabilities in the wake of islands and modify the features of motion into the Caribbean (Jouanno et al. (2009), citerichardson2005caribbean).

- Simmons and Nof (2002) suggested that smaller NBCr ($L/R_i = 0.5$) are broken up by the islands originating smaller offspring eddies or "shear flow streamers" that can be squeezing across the passages between the island (Murphy et al., 1999), where R_i is the radius of ring and L the scale of the island. Counter-intuitively, larger eddies ($L/R_i = 0.3$) are pushed into the Caribbean Sea as coherent structures, specially if they collide with the relatively smaller islands.

- Another work demonstrates that Atlantic Rossby Waves can pass through ocean barriers such as the Lesser Antilles (pedlosky2001Rowaves).

- The eddies into the Caribean are embedded, intensified and grown in the sCC due to presence of instabilities along basin. This can enhance the Eddy Kinetic Energy without the presence of NBCr in the east of Lesser Antilles (Jouanno et al., 2009).

- The meridional migration of Inter-Convergence Tropical Zone regulated the intensification of wind-stress curl (Jouanno and Sheinbaum, 2013) and sea surface temperature (Bernal et al., 2006). It had been proposed as the source of energy for the mesoscale motion in the Caribbean as happen in the upwelled filaments in the Guajira Peninsula.
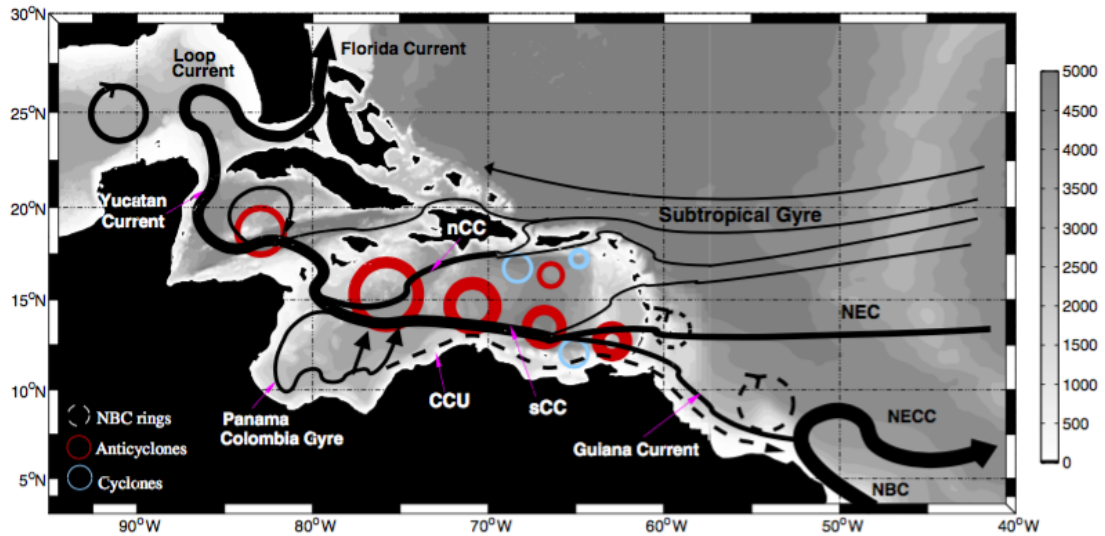
Figure 2.1: Illustration of the main mesoscale features and current paths of the Caribbean Sea and its surroundings (Extracted from Jouanno et al. (2008))

- Baroclinic (BC) Instabilities appear in the sCC and some upwelling spots of the coastal of Venezuela and Colombia, whereas and Barotropic (BT) Instabilities appear in the Cayman basin.

- The anticyclon eddies merged in the sCC are dominants and most stronger than the cyclonic eddies in the north of the basin and the cyclonic Panama-Colombia gyre. This latter, might help to enhance the EKE in the Guajira Peninsula, since is the origin of the Caribean Coastal Undercurrent (CCU).

- Anticyclonic Eddies and sCC continue move toward the Cayman Basin inducing transport and vorticity fluctuations in the Yucatan Channel, tending to delay the pinch off the Loop Current and shedding the anticyclonic eddies in the Gulf of Mexico (Oey et al., 2003)

- Finally the Loop Current cross the Florida Channel and feels the β effect, intensifying the flow and forming the Gulf Stream alongshore the USA coastal.

2.2 Model and configurations

We used the Regional Ocean Modelling System (ROMS); (Shchepetkin and McWilliams, 2005)). Our simulation has a parent grid whose domain spans from $5°S$ to $32°N$ and from $99°W$ to $60°W$ with a resolution of 6 km, sufficiently large to reproduce the meso- and large scale dynamics in the region such as the retroflection of the North Brazil Current (NBC) and its anticyclonic eddies, the growth of the eddies the Caribbean Sea, the Loop Current and its retroflection on Gulf of Mexico and the outset of Gulf Stream. A nesting grid is implemented with a resolution of 3 km and a domain that extends from the east of the Lesser Antilles to the Nicaraguan Coast $[84°W - 36°W]$ and from the coast of Venezuela and Colombia in the south to the Haiti-Dominican Republic Island to the north [5 °N - 19 °N] (Fig.3.1). Both domains contain 32 terrain-following vertical levels with increasing resolution towards the surface.

The initial and boundary conditions used for the physical variables were obtained from a climatology of the Simple Ocean Data Assimilation (SODA) (Carton and Giese,2008). The model is forced at the surface with climatological winds from QuikSCAT (Risien and Chelton, 2008) and heat and freshwater surface fluxes from the Comprehensive Ocean-Atmosphere Data Set (COADS). The topography used used is the database from NOAA-NGDC (ETOPO1) which has a resolution of $1'$.

The model simulation started from initial conditions, boundary and surface forcing from 1998 and the parent grid was spun up for 3 years. Subsequently, the nested domain was initialized from an interpolation of the parent domain and spun up for 2 more months before the diagnostic period (2001-2002), from here on the numerical simulation has attained statistical equilibrium in both domains. The model was integrated for three more years, saving the instantaneous values and two-day averages of all physical variables. Our analysis focuses on three specific regions, namely the Colombia (Col), Venezuela (Ven) and south-east of the Lesser Antilles (Rings) basins as shown in Fig.

Figure 2.2: Model domain range ($6km$) and nesting grid($3km$) (dashed rectangle) and areas where we computing the spectra analyse and other calculus (small boxes): Colombia Basin (Col), Venezuela Basin (Ven) and Rings Basin (Rings)

3.1.

2.2.1 Validation of the simulation

As part of validation of the simulations, we compare the modelled SST with the satellital sensor Advance Very High Resolution Radiometer (AVHRR) Pathfinder (Casey et al., 2010) in two opposed seasons of the year 2001. First in the boreal winter and second in the summer (see in the Appendix A Fig.1), since the variation of SST in the region is due primarily to the meridional and seasonal migration of Inter Tropical Convergence Zone (ITCZ). In general, ROMS exhibits small or almost null difference with the AVHRR in our areas of study, only a colder bias at the CUS along the Venezuela and Colombia coastal for both seasons. It can generate that ours analyses are overestimated, because as increasing the resolution of model as increase the turbulence and increase

of the same way the vertical velocities that bring cool water of subsurface. Another regions exhibit most difference as the Gulf of Mexico and Gulf Stream, notice that this difference of SST is higher in the winter season.

For evaluate temporally the cooler bias around of our areas of study, Fig. 2.3 shows the annual variation of SST around the Lesser Antilles. There can notice a bias between the model solution and satellite observation, being higher in the winter period (Dec-Feb) when the wind stress are more strong (see in the Appendix A Fig. 2). The longitudinal and temporal variability of SST from two same source are consistent in phase and intensity. Also is relevant to notice that the higher values of anomalies (panel bottom-left) occur in the leeward of the islands, due to increase in turbulent circulation by the shear flow that across the channels.

2.3 General and Specific objectives

Evaluate the variability of submesoscale dynamic in the Caribbean Sea, analysing the influence of the North Brazil Current Rings, the topographic interaction and the wind stress effect in the region.

- Identify the main physical factors that interacts in the submesoscale dynamic of Caribbean Sea.

- Quantify the energetic transference between scales inside of Caribbean Sea and the upstream of the Lesser Antilles.

- Determine the effect of restratification of mixed layer due to submesoscale dynamic in the Caribbean Sea.
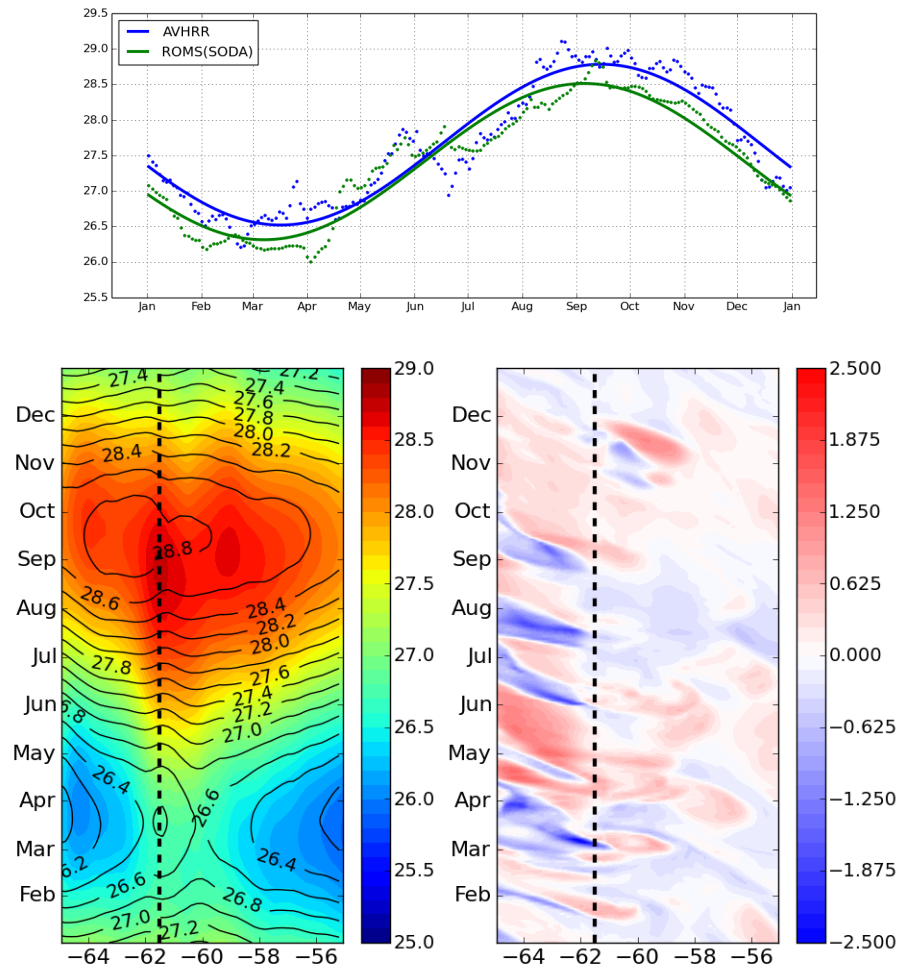
Figure 2.3: Sea Surface Temperature (SST) in a zonal section averaged between the $12°N$ and $14°N$. It crosses the Lesser Antilles between the $55°W$ and $65°W$. (Top) The dots are SST spacial averaged for each two days and the line is the temporal tendency computed with least square from AVHRR (blue) and ROMS simulation data (green). (Bottom) Longitude-time section composite seasonal cycles of SST from AVHHRR (colors) and model (contours) in the left panel and the anomalies from model simulation respect to least square tendency in the right panel

Chapter 3

Manuscript

3.1 Introduction

The Caribbean Sea is a semi-enclosed basin confined in the east by the island chain of the Lesser Antilles and in the west by the Yucatan Strait. Its main current is the south Caribbean Current (sCC), this is derived from the shear flow of the North Equatorial Current (NEC) across the channels between the islands, continuing the surface circulation toward the Gulf of Mexico and closing the North Atlantic Subtropical Gyre (Johns et al., 2002). Mesoscale eddies are ubiquitous in the Caribbean and increase their size while they move westward, resulting in enhancing Eddy Kinetic Energy (EKE) along the basin (Jouanno et al., 2012). Thereby, the mesoscale dynamics of the Caribbean generates and transports energy toward the Yucatan Strait, influencing the dynamic of the Loop Current and the shedding of anticyclones eddies in the Gulf of Mexico (Oey et al. (2003);Athié et al. (2012)) and potentially being the genesis of the western boundary current of the North Atlantic ocean which ultimately becomes the Gulf Stream.

In terms of submesoscale dynamics, two regions within the Caribbean Sea are of potential interest. The lee of the Antilles, where eddies and filaments result from
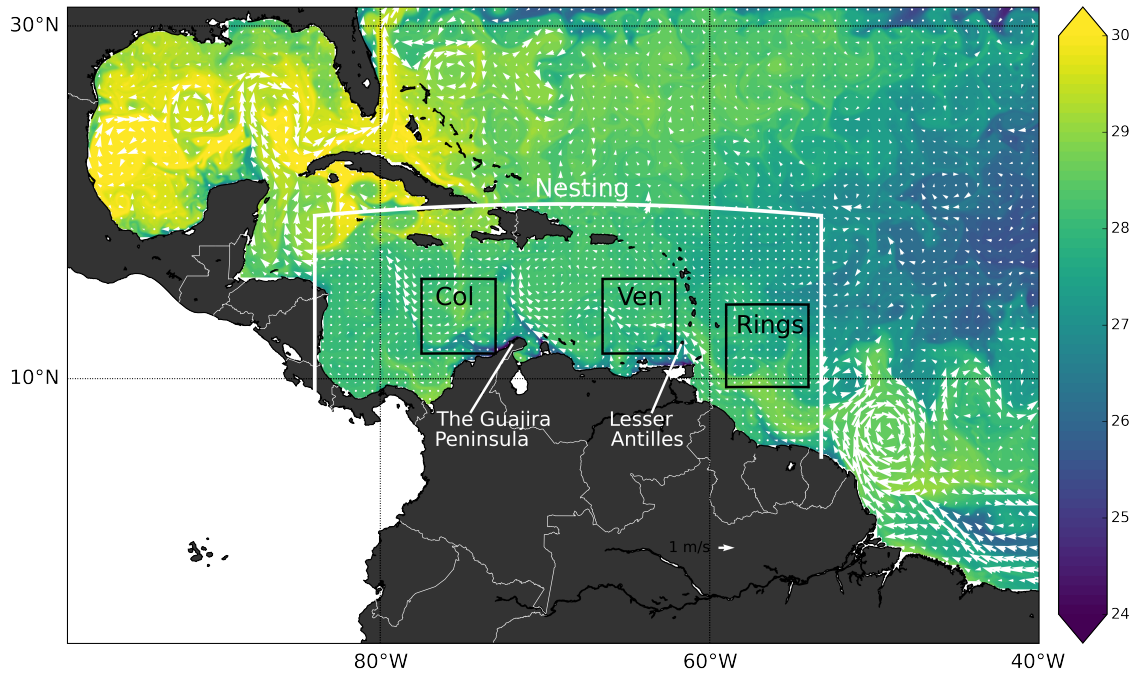
Figure 3.1: Average SST and velocity field of two days in July for the parent domain that has a resolution of $6km$ and the nesting grid of $3km$ as show the white box.

the interaction between the North Equatorial Current Rings (NBCr) and the islands (Fratantoni and Richardson, 2006), and the Caribbean Upwelling System (CUS), which results from the interaction between the winds from the Caribbean Low Level Jet (CLLJ) and the coast, giving rise to filaments that transport coastal waters offshore (Andrade and Barton (2005);Rueda-Roa and Muller-Karger (2013)).

Intense heat flux generates a highly stratified region where the exchange between the mixed layer and the thermocline is hindered. Regions of submesoscale motions could facilitate this exchange of tracers by enhancing of vertical velocities between the mixed layer and the thermocline (Fig. 3.1).

Mesoscale structures may interact with the filaments and advect them into the interior. The filaments are stretched, surround by the eddies which leads to increased density gradients, disrupting the thermal wind balance, generating ageostrophic secondary circulations (Capet et al., 2008b). This instantaneous and turbulent flow tries

to break up the mesoscale structure and the base of mixed layer. Thus, the interaction between mesoscale and submesoscale dynamics have the role of stir and mix the lateral gradients and reduce the vertical gradients of tracers and momentum, respectively, with the aim of re-stratify the mixed layer (Boccaletti et al., 2007).

Jouanno et al. (2009) suggest that baroclinic instabilities in the upper layers of the Caribbean can occur on short time scales, similar to the Gulf Stream, and this very short BC time scale is associated with a strong vertical shear in the upper 100 m depth. Jouanno et al. (2012) quantified how much the first baroclinic (BC) and barotropic (BT) modes of instabilities could influence the seasonal and the zonal modulation of EKE in the Caribbean Sea, being more relevant the BC mode in the Colombia region. This is consistent with theoretical work of Scott and Wang (2005) which shows how BC instability converts potential to kinetic energy, and hence appears as a source for KE, whereas the BT instability could to be linked with the possibility to add or remove these KE from larger scales. Therefore, on the vicinity of the Lesser Antilles domain the events of dissipation of NBCr by conversion from KE to PE, i.e. by BT instability, whereas on the Guajira Peninsula BC instabilities allows the enhancing of EKE.

An analysis of scales reveals that the energetic instabilities of the mesoscale dynamic are larger than the dissipation effects of the smaller scales, so there should exist a range of scales where neither forcing nor dissipation terms are explicitly important to the dynamics. This range may be defined as submesoscale regime, where the nonlinear terms are dominant in the momentum balance (Vallis, 2006). In this range the energy embedded in the mesoscale is transferred to the smaller scales, through the submesoscale dynamics (Capet et al., 2008a), where the ageostrophic velocities trigger the frontogenesis, which can be solved by the Quase-Geostrophic (QG) and by Semi-geostrophy theories (Klein et al., 2008). This dynamics are easy to identify with the Rossby Number $R_o = \zeta/f$ is $O(1)$, where $\zeta = U/L$, U is the scale of the horizontal velocity and $L = U/f$ determine the length scale, so the horizontal range of subme-
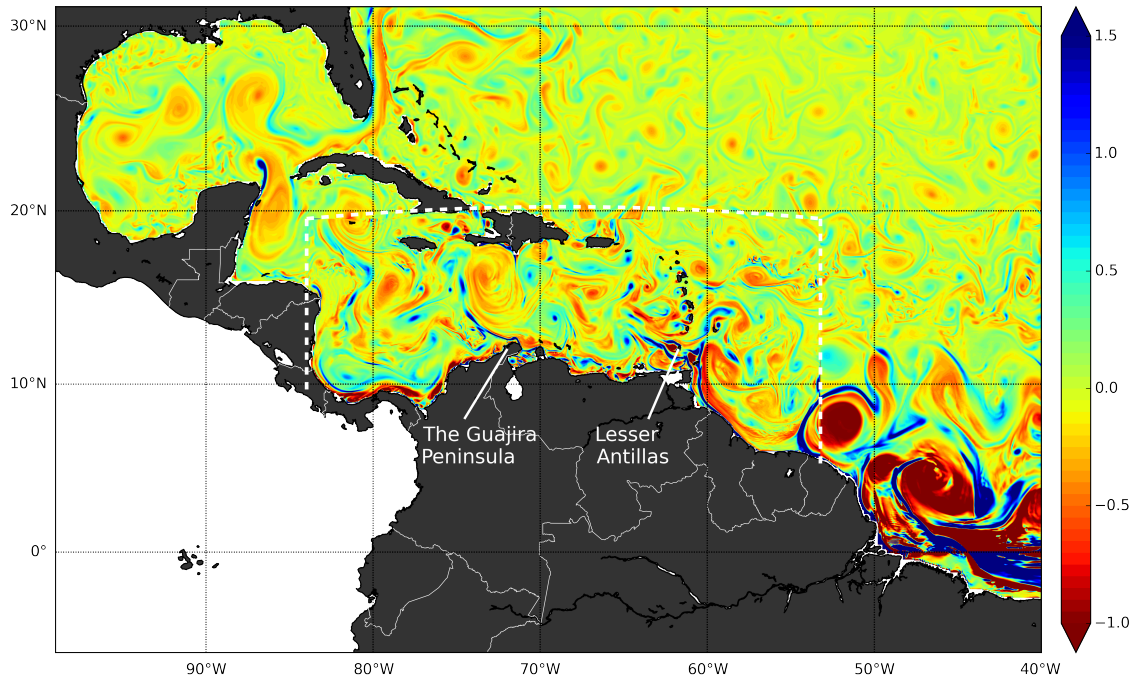
Figure 3.2: Rossby Number $R_o = u/Lf$, as balance of relative and planetary vorticity. Look that for $R_o >= 1$ the inertial terms take the same importance of coriolis parameter in the quase-geostrophy theory

soscale $O(1)km$ is smaller than mesoscale of $O(100)km$, vertical scale of $O(10)m$ and time scale of $O(1)day$. Mesoscale structures are usually associated with $R_o << 1$ and are surrounded by $|R_o| \geq 1$ wich shows the importance of nonlinearity at the edges of mesoscale structures and upwelled filaments as can sees in the vicinity of the islands and the Guajira Peninsula respectively (Fig. 3.2). The balance between the nonlinear terms and the geostrophic terms, near these regions, allows the transference of energy and leads to the dissipation or forcing processes intrinsically. This is achieved through thermal wind imbalance and the generation of ageostrophic secondary circulations (ASC) across the front, which induces the lateral mixing and subsequent re-stratification of the upper ocean.

Frontogenesis is the main mechanism which favours the emergence of instabilities that result from the evolution of the mesoscale. High lateral strain rate due to the

nonlinear interaction of the lateral velocity shear and buoyancy gradient acts to re-stratify the mixed upper ocean. This is not the only way to have sumesoscale dynamics, since unforced instabilities from ageostrophic flow, like the shear flow enhancing the vertical fluxes on the island wakes, hastens the slumping of fronts and get more faster restratification than the mesoscale BC instabilities (Thomas et al., 2008).

Most of the previous research in submesoscale dynamics focuses on regions with larger density gradients in the Eastern Boundary Upwelling System as California and Peru (Capet et al. (2008a); Penven et al. (2005)), in western boundary currents such as the Gulf Stream and Western Subtropical Pacific (Callies and Ferrari (2013); Qiu et al. (2014)). To quantify the submesoscale dynamics in these regions, in situ observations and computer simulations at high resolution were use in mid-latitudes where the gradient of temperature is higher than in tropical latitudes and the turbulent effects are more intense. This does not preclude the importance of submesoscale processes in the tropical and stratified ocean.Marchesiello et al. (2011) demonstrated the influence of submesoscale processes on the equatorial upwelling in the Central Pacific Ocean where tropical instability waves are generated. They show that the submesoscale range is shifted towards larger spatial scales than the in mid-latidudes. This results from the fact that the Rossby first baroclinic deformation radius L_D increase in the tropical latitudes.

Although the Caribbean Sea is not characterized, as a whole, by strong density gradients, the two regions that are the focus of this study, namely, the CUS and the Lesser Antilles, are associated with upwelling and vorticity filaments within which submesoscale processes may play an important role. In this work we aim to show that the possible action of submesoscale dynamic through frontogenesis by stirring of filaments in the Guajira Upwelling and by unforced ageostrophic baroclinic instabilities in the leeward of Lesser Antilles (Fig. 3.2) that tries to re-stratify the mixed layer of the Caribbean.
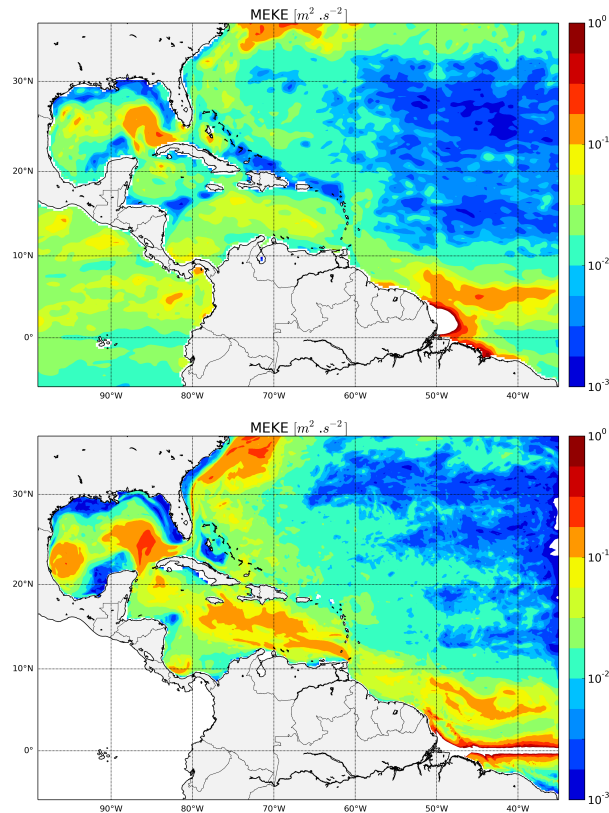
Figure 3.3: Mean Eddie Kinetic Energy compute with anomalous velocities from AVISO (top) and output of simulation (bottom) for the year 2001

The goal of this work is to show how submesoscale dynamics are present in the turbulent circulation of the Caribbean Sea, observing the transference of energy from mesoscale anticyclonic NCBr to smaller spatial scales, assessing their influence on the KE enhance along the Caribbean basin and how can this submesoscale processes are activated, influenced and undergoes by the dominant mesoscale flow along the basin.

3.2 Mesoscale Circulation

The sCC is the continuation of the wind-driven flow of the subtropical gyre as the current passes through the gaps of the Lesser Antilles. This vertically and horizontally sheared flow is disturbed due the input, due to input of anticyclonic vorticity by the

arrival of NBCr near the islands. Depending of the size the NBCr in relation to the island, it is broken up and generates smaller eddies in the lee of the island (Simmons and Nof, 2002) that are embedded by the sCC. Inside the Caribbean, increased eddy activity is observed in the vicinity of the Guajira Peninsula. Jouanno et al. (2009) suggest that the sCC has the same values of baroclinic time scale (BTS) as the Gulf Stream, defining BTS as the time for which the mean flow could develop BC instabilities. They find that the Guajira Peninsula and the wake side of the islands are the regions with the lowest values of BTS and suggest that these two points are the main source of EKE in the region due to these instabilities.
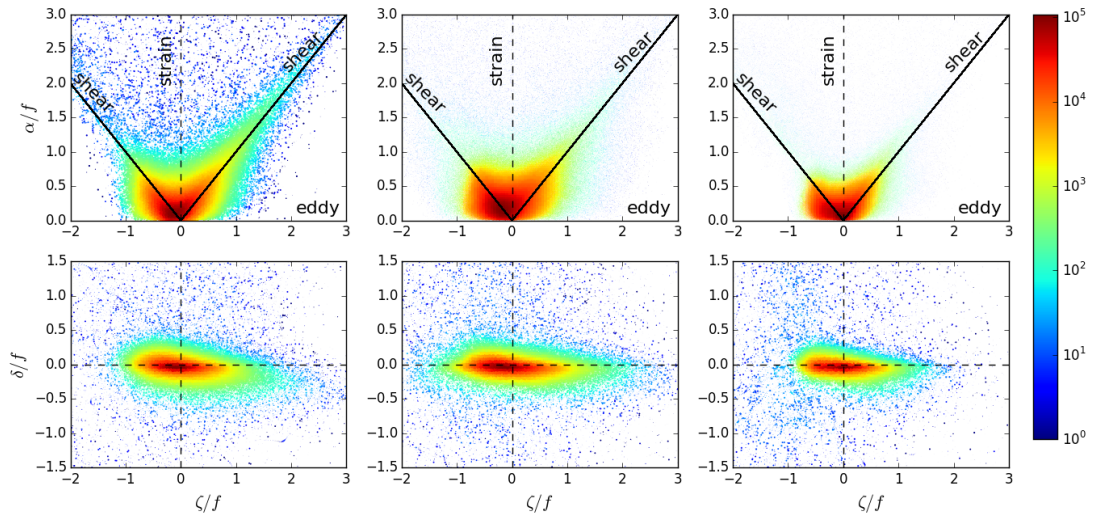
Figure 3.4: Joint probability distribution function (JPDFs) of pairwise of vorticity and strain rate (top) and vorticity and divergence (bottom) in 10 m of depth. The left column corresponde to the Colombia basin, the center to the Venezuela and the right to the Rings basin. Black 45° in the top panels indicate the one-dimensional shear flow ($\alpha = |\zeta|$). All terms are normalized by the coriolis parameter f of each latitude.

The model reproduces fairly well the mean features of superficial circulation around the Caribbean Sea (Fig. 3.1). A comparison between the remotely observed EKE from AVISO and our simulated EKE shows that the model correctly reproduces the variability in the region (Fig. 3.3). A slight overestimation is seen in the model results.

This is attributed to the increased model resolution when compared to the satellite product. Nevertheless, the model correctly reproduces the gradual rise of EKE along the Caribbean as suggested by Jouanno et al. (2012). Note also the increase of EKE in the retroflexion the NBC that pinches off large, isolated warm-core rings, exceeding 450 km in diameter, move toward northwestern, decreasing its EKE along the path toward the Lesser Antilles (Fratantoni and Richardson, 2006). Small eddies cross or are created in the lee of the island interact with mesoscale structures and are dragged by sCC into the Caribbean basin (Jouanno et al., 2009). EKE increases westward due to BC instabilities originated in the CUS on the Venezuela and Colombia's coast (Jouanno et al., 2012). Downstream, can see the higher EKE in the Loop Current and mesoscale eddies in the Gulf of Mexico and the intensification of the western boundary current system which will ultimately become the Gulf Stream.

The transition between the mesoscale and submesoscale occurs primarily due to the increase of the relative vorticity $\zeta^z = \partial_x v - \partial_y u$. When $|R_o| \sim 1$, nonlinear terms become important as to be comparable with the planetary vorticity (i.e., $|\zeta^z| \geq f$) as shown in Fig. 3.2. High Rossby number occurs primarily on the edges of mesoscale eddies or fronts, where the strain rate is high (i.e. $\alpha = [(\partial_x u - \partial_y v)^2 + (\partial_x v + \partial_y u)^2]^{1/2} \geq f$), while the mesoscale regime is dominated by the planetary vorticity f. We compute the joint probability distribution function (jPDF) of the vertical vorticity (ζ^z), strain rate (α) and divergence (δ) for our finest numerical solutions of 3 km (Fig .3.4). The anticyclonic vorticity has a larger jPDF than cyclonic vorticity in all areas. This occurs where the mesoscale dominates (i.e. $\zeta^z/f << 1$) as expected into the solid body rotation like eddies. However the Colombian basin also shows higher values of cyclonic vorticity jPDF ($\zeta^z > 0$ and $R_o \geq 1$) when compared to other areas, which indicates the action of submesoscale turbulence (Shcherbina et al., 2013). This strong positive vorticity is associated with high strain rate and approached a pure shear relationship $\alpha = |\zeta|$ indicating that the cyclonic vorticity occurred predominantly over the fronts

or filaments of the Guajira Upwelling. Also, notice that Venezuela basin have lesser but considerable probability to develop this same vorticity dynamic, in contrast with the "Rings" area that is dominated by mesoscale vorticity. The model predicts neutral divergence in all areas of study, with a slight increase of divergence associated with the enhancement of EKE into the Caribbean sea.

3.3 Submesoscale Dynamics

3.3.1 Evidence of Frontogenesis in the Caribean Sea

Frontogenesis starts with the disruption of the thermal wind balance, high ageostrophic velocities are generated in order to reduce the strong density gradient and are accompanied by the upward velocities on the light (warm) side and downward on the heavy (cold) side (Capet et al., 2008b). This phenomenon is a consequence of the increase of density gradients on elongated filaments, developing ASC across the fronts on smaller scales, stirring the filament and together with the shear vertical velocities turn and slump the isopycnals of the front, attempting to recover the thermal wind balance. In the ocean, these processes occur essentially on the submesoscale range. They trigger the turbulent isotropization and the forward KE cascade.

In order to demonstrate the influence over tracer fluxes and the restratification promoted by submesoscale processes, Fig. 3.6 shows the zonal and time average divergence of the vertical heat flux $-\partial_z \overline{wT}$, divergence of the horizontal eddy heat flux $-\nabla_h \overline{U_h T}$ and divergence of the buoyancy flux $-\partial_z \overline{wb}$ where $b = -g\rho/\rho_o$ over the boundary layer influenced by the Guajira Upwelling in the Colombia basin [76.5 °W - 73.0 °W and 11.5 °N - 14.9 °N]. We separated each variable (V) in its mean ($\overline{V}$), mesoscale (V') and submesoscale (V'') components after to apply its respective filter as:

$$V = \underbrace{\overline{V}}_{} + \underbrace{(\tilde{V} - \overline{V})}_{} + \underbrace{(V - \tilde{V})}_{}$$

$$mean + meso + submeso$$

(3.1)

Where $\overline{V}$ is the one year average and $\tilde{V}$ is obtained by applying a high-pass filter with a horizontal smoothing of 3 and 5 points of grid for the solution of $6km$ and $3km$ respectively, following the methodology of Capet et al. (2008a). So, we get to separate the velocities in mean. meso and submesoscale and we can see the order of each one of these in the next figure:
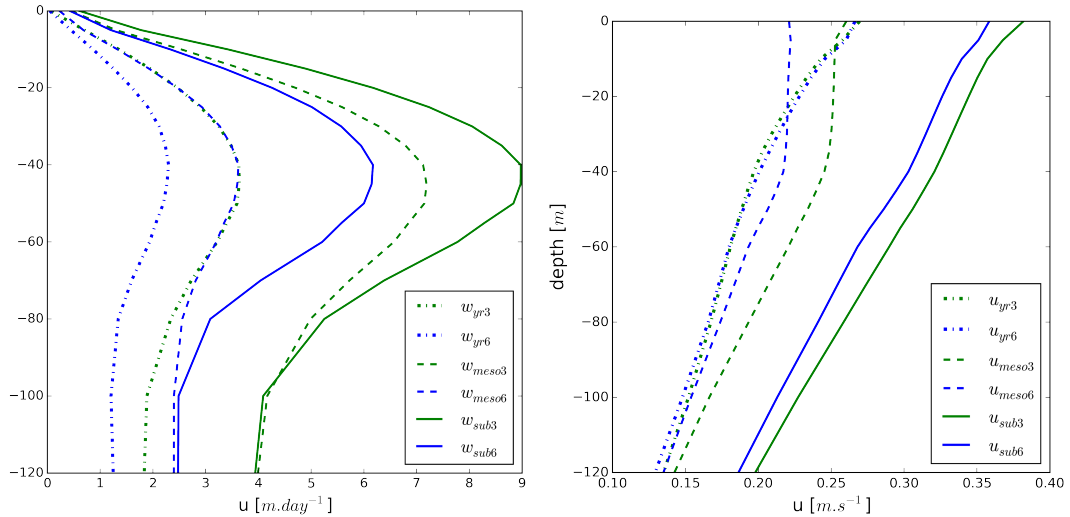
Figure 3.5: Vertical and zonal (left and right) velocities profile after of mean (dot-dashed), meso (dashed) and submesoscale (continuous) for two solutions of 3 km (6 km) in green(blue).

The divergence of heat flux for the submesoscale $\partial_z \overline{w''T''}$ acts to re-stratify the mixed layer (first row in Fig. 3.6) by warming above and cooling below, being more intense in the vicinity of the Guajira. However the mesoscale flux $\partial_z \overline{w'T'}$ (second row), is dominant as compared to the submesoscale in the process of restratification between the isotherms $26°C - 27°C$ in the vecinity of the Guajira upwelling. Notice that

the submesoscale heat flux is dominant in the costal upwelling regions $(11.5°N)$ and presents a countergradient flux, cooling the surface and warming the ocean interior, due to the lateral transport of Caribbean Coastal Undercurrent (CCU) in this latitude. The increment of resolution slightly enhances the heat flux, and at the same time enhance the restratification within the mixed layer. On the other hand, both the meso- and submesoscale componentes of the horizontal eddy flux $\nabla_h U_h T$ (third row) is important in the advection of heat in the region, being larger than the vertical eddy flux. At the same time, $\nabla_h \overline{U_h T}$ is larger in the mesoscale decomposition, so it hinders any restratifycation away of the upwelling zone. The buoyancy flux profile $-\partial_z \overline{wb}$ (latter row) confirms the enhancement of vertical velocities in the upwelling area influenced by the wind. See also the enhancement with the increment of grid resolution. This proves that these upwelling processes develop the most exchange of properties between the mixed and the pycnocline layer in the Colombian basin, and together with the CCU, increase the probability of generation of BC instabilities that increase EKE in the circulation of the region, as suggested by Jouanno et al. (2012).

Additional evidence of the presence of frontogenesis in the Caribbean Sea is the rate of increase for the horizontal density gradient (F_s) arising from the straining by the horizontal velocity field. This allows localized regions where the ageostrophic velocities are induced due to the frontogenesis process, just where F_s is large (Capet et al., 2008b):

$$F_s = Q_s \cdot \nabla_h \rho \tag{3.2}$$

where

$$Q_S = -\left(\frac{\partial u}{\partial x} \frac{\partial \rho}{\partial x} + \frac{\partial v}{\partial x} \frac{\partial \rho}{\partial y}, \frac{\partial u}{\partial y} \frac{\partial \rho}{\partial x} + \frac{\partial v}{\partial y} \frac{\partial \rho}{\partial y} \right) \tag{3.3}$$

Fig. 3.7 displays the main patterns around the fronts and filaments as well as are the instantaneous values of vertical velocity w, the density gradient $|\nabla_h \rho|$, the divergence of heat flux $w''T''$ and the previously defined F_s into the Caribbean Sea (top). The

most intense features appear associated with the filaments of the Guajira Upwelling and sheared circulation leeward of Lesser Antilles. It also shows a change of sing of w on each side of the front in the first region. Intensification of vertical velocities are localized on the boundary layer,potentially enhancing the exchange of tracers between the mixed layer and the pycnocline (bottom). The more intense heat flux is associated to smaller filaments in the Guajira Upwelling and the horizontal shear flow in the wake of the Lesser Antilles. Notice also how this flux of heat remains in the boundary layer, inducing restratification near the filament and while being much smaller away from this regions.
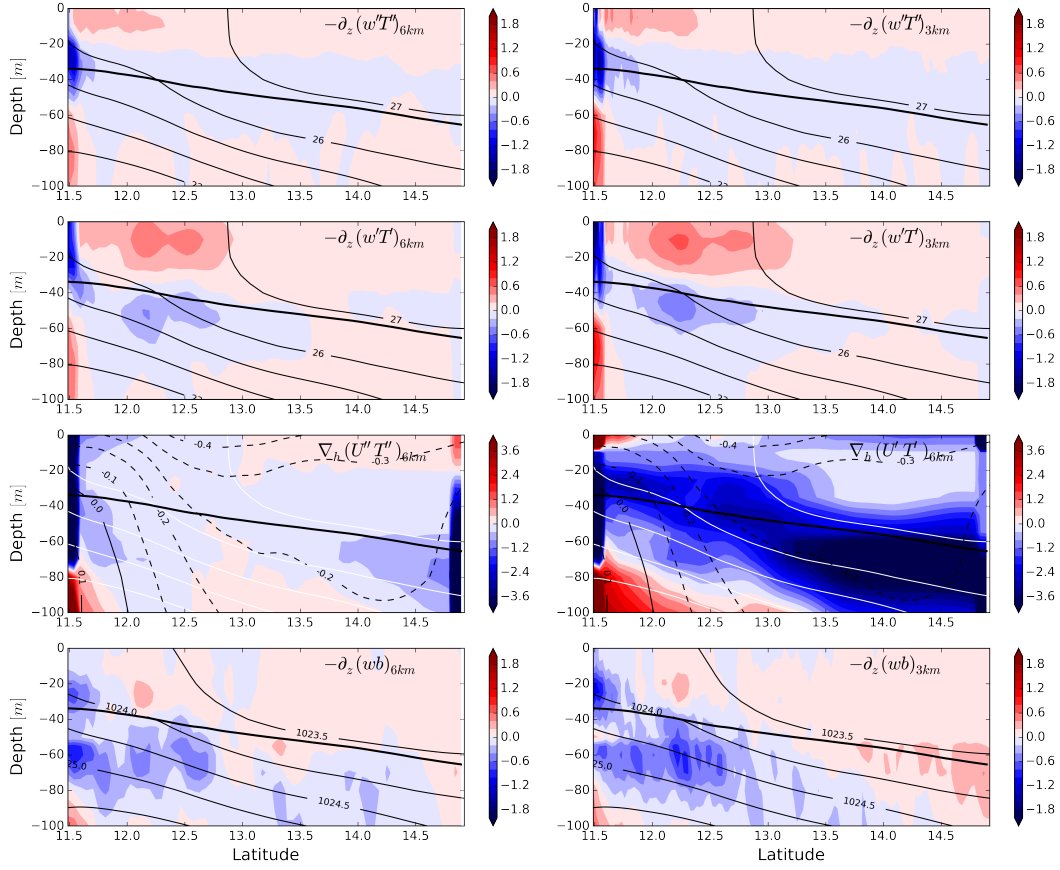
Figure 3.6: Sections of time and zonal averaged vertical eddy flux divergences of heat $-\partial wT$ $[10^{-6} \, °Cs^{-1}]$ for submesoscale and mesoscale after the respective filter (first and second rows), horizontal eddy flux divergence of heat $-\nabla_h u_h T$ $[10^{-6} \, °Cs^{-1}]$ (third row) and buoyance flux $-\partial wb$ $[10^{-9} m^2 s^{-3}]$ (last row). The black line show the boundary layer depth $\overline{h}(y)$. The contours in the two first rows represent the mean isoterms, while in the third row contours display the year mean zonal flow u (dashed line are the negative velocities) and white line the isoterms, for the buoyance flux the contour are the isopycnals.
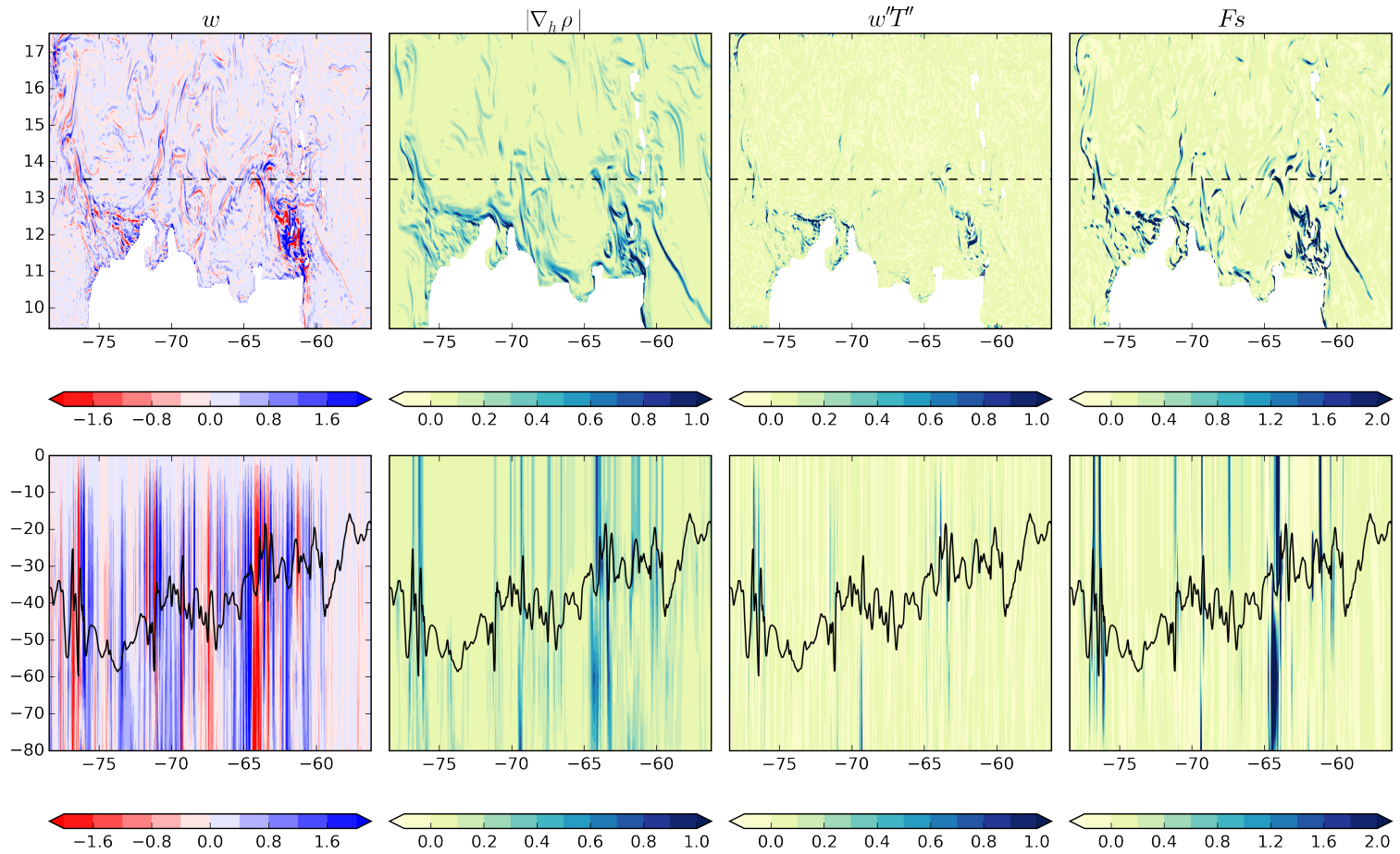
Figure 3.7: Instantaneous patterns that demonstrate the presence of submesoscale regimen in the Caribbean Sea: vertical velocities w $[10^{-4}m.s^{-1}]$(first column), density divergente $|\nabla_h\rho|$ $[10^{-5}kg.m^{-4}]$ (second column), flux divergence $w''T''$ $[10^{-5}m°Cs-^{-1}]$ (Third column) and rate of increase of horizontal density gradient F_s $[10^{-4}kg^2m^{-8}s^{-1}]$ (last column). In the top are the horizontal patterns in $10m$ depth and bottom are the vertical patterns

3.3.2 Turbulence and KE Spectral Analysis

Mesoscale dynamics in the upper ocean is primarily two-dimensional. This is a consequence of the dominant effect of rotation and stratification, which make horizontal processes larger and prevent vertical motion. All energy contained in the horizontal and larger scales has to be transferred toward three-dimensional dissipative scales, where isotropic effects doing possible this transference of energy. QG-turbulence theory predicts the KE transference toward smaller scales via the forward energy cascade, although we need to be careful with the important ageostrophic corrections. Depending on the stratification, in upper ocean with a weakly stratified layer presents a flatter KE spectrum than a deeper, mixed layer where the KE transfer occurs with a steeper slope (Callies and Ferrari, 2013). Thus, an the upper ocean with constant stratification the submesoscale inertial range is relatively flat (i.e. $k^{-5/3}$), allowing the transference of energy to larger scales and enstrophy to smaller scales near L_D. While for an ocean with a deeper mixed layer this same inertial range falls off steeply with a slope k^{-3} transferring potential enstrophy by forward KE cascade for into small scales.

Thereby, there are two key issues in the analysis of KE spectral through of the 2-D turbulence: barotropic flow induces an inverse energy cascade from scales close to LD to larger scales while enstrophy is transferred from large to small scales (Klein et al., 2008). This is similar to the manner as the energy is transferred to smaller scales in isotropic 3-D turbulence (Vallis, 2006). The transference of energy and enstrophy occurs through an increase of the vorticity gradient in the stretching of eddies and filaments. This defines the limit between the inertial range of energy and enstrophy, making evident the length scale where stirring begins to act. This limit is noticed in the change of slopes from $k^{-5/3}$ to k^{-3} in the KE spectrum such as in Fig. 3.8. Therefore, the only way to determinate the transfer rate of energy or enstrophy is through the high-resolution measurements or computational simulations that reproduce the isotropic turbulence in the interior of the ocean.

The computation of the two-dimensional KE spectrum of the horizontal velocity field (u,v) was done over three specific regions of Caribbean Sea that seem to be dynamically different. The first is the east of Lesser Antilles where KE from NBCr is dissipated and transferred toward smaller scales. The second is the lee of the islands in the Venezuela basin where an increase in EKE is observed due to lee eddies that are formed in the region. The last regions is the Guajira Upwelling in the Colombia basin, where the interaction between upwelling filaments and anticyclonic eddies generate the largest EKE in the Caribbean Sea. These three regions are delimited in Table 3.1, each covers an area of $(384km)^2$ as illustrated in the boxes of Fig. 3.1. The spectral decomposition is based on 2-D fast Fourier transform of the anomalies of two-day averaged velocity fields (179 time steps which correspond to a year of model output) and averaged temporally later, applying a 2-D Hanning window smoothing in the boundaries values.

Table 3.1: Delimited areas for Fourier Analysis in the KE Spectral: The number of point in the fft analysis varied according to resolution: 64 point for $6km$ and 128 to $3km$

	Latitudinal Range		Longitudinal Range	
Region	Low	Up	Left	Right
Guajira Upwelling	$11.5°N$	$14.9°N$	$76.5°W$	$73.0°W$
Island Wakes	$11.5°N$	$14.9°N$	$65.5°W$	$62.1°W$
Rings decompose	$10.0°N$	$13.4°N$	$59.0°W$	$55.0°W$

Despite the increased resolution of the model grid from 6 km to 3 km, the KE spectrum of both solutions does not converge toward the slope of k^{-2} (Fig. 3.8) as in the California Current System Capet et al. (2008c) and in the tropical instability waves in the Pacific Ocean Marchesiello et al. (2011). However, for the three areas and for the two solutions have shallower slopes $K^{-5/3}$ at smaller wavenumbers $k < 3 \times 10^{-5}[m^{-1}]$ correspondent to larger scales $\lambda > 200km$ in which the mesoscale dynamics is dominant. For $k > 3 \times 10^{-5}[m^{-1}]$ the spectrum starts to fall off steeply with a slope of k^{-3} keeping the convergence to this slope until the dissipative scales. This result is consistent with
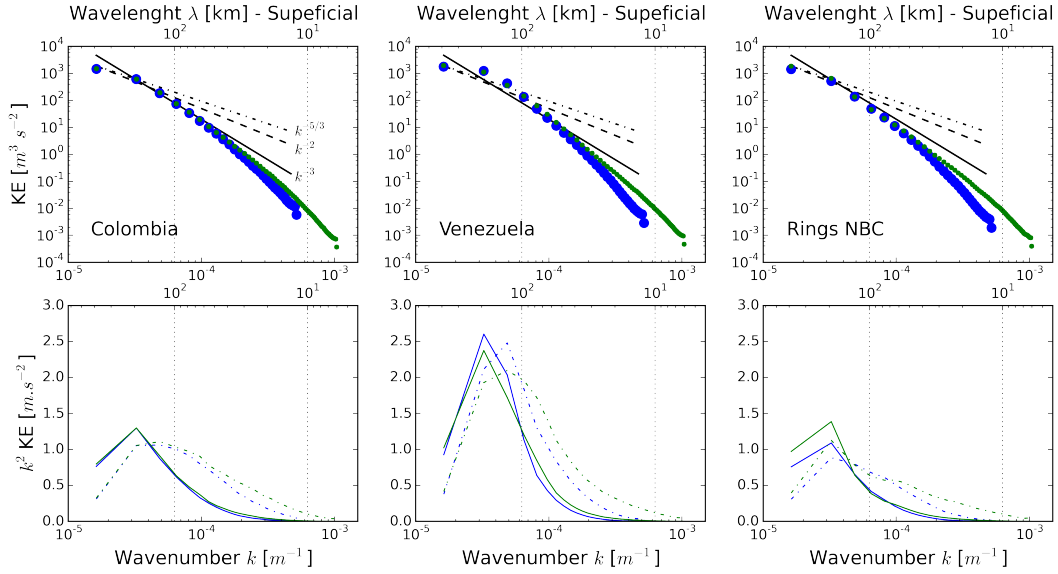
Figure 3.8: Top: KE spectra in function of wavenumber and horizontal velocity (u,v) in 10 m depth for resolution grid $6km$ and $3km$ (blue and green respectively) in the Guajira Upwelling (left), Venezuela (medium) and rings of NBC (right) basin. Bottom: Spectrum multiplied by k^2 representing the enstrophy inertial range, solid line correspond to multiplied by k^{-2} and straight lines by k^{-3}

the suggested about the effect of the stratification in the EK cascade, in our case, the mixed layer of Caribbean is depth and allows large isotropic processes and consequently can extract more KE. The largest differences between the two solutions is seen in high wavenumbers as the dissipative range is shifted toward smaller scales of the order of twice the resolution.

At the upper row of Fig. 3.8 the KE spectra at 10 m depth was similar for all three regions, only in the Venezuela basin the KE appear to be slightly higher than the other areas around of scales of $120km$ $k = 5 \times 10^{-5}[m^{-1}]$. This is most notable in the bottom panels that show the compensated spectrum for k^{-2} (solid lines) and k^{-3} (dashed lines), which allows to locate the inflection point between the two slopes and determine the inertial range of the energy cascade and the inertial range of the enstrophy in QG turbulence, respectively (Capet et al., 2008c). Notice the solid lines in all panels show a peak of energy around $k = 3 \times 10^{-5}[m^{-1}]$ falling strongly as k increases until its
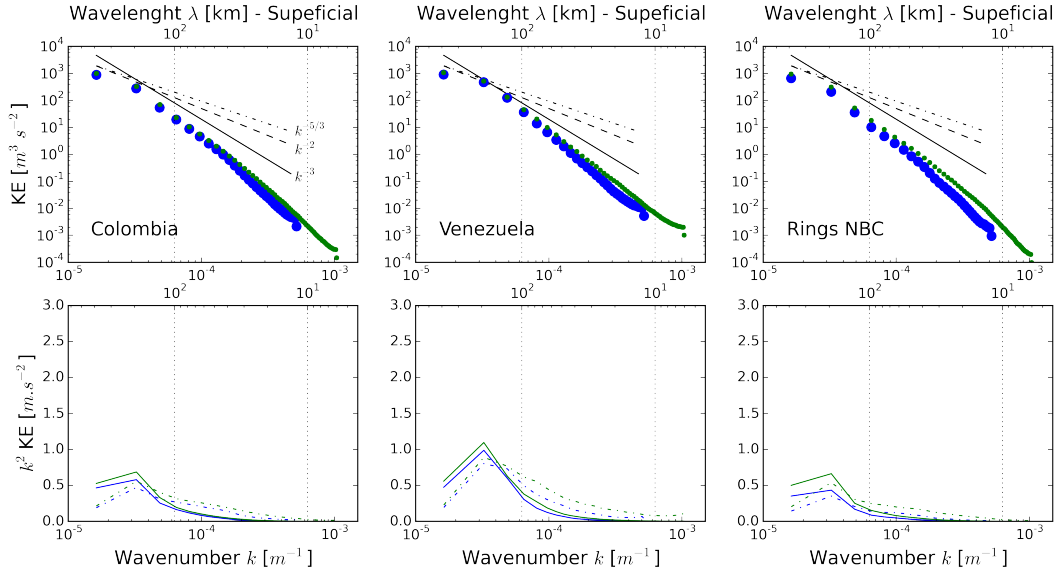
Figure 3.9: Equal that Fig. 3.8 but for the 80 m depth.

flattening out in the dissipative range. On the other hand, the dashed lines have a flat interval between 200-80 km ($3 \times 10^{-5}[m^{-1}] > k > 6 \times 10^{-5}[m^{-1}]$) approximately inside the Caribbean, that correspond to the submesoscale inertial range where the potential enstrhophy is then cascaded downward to smaller scales into the Caribbean Sea. Note that this does not occur in the "Rings" region. This could be the limiting length scales of dynamic processes than inject energy to higher scales or transferring cascade energy to smaller scales as seen below.

KE spectra in the pycnocline (80 m depth) are similar to the ones in the surface layer, but which slightly lower KE. These also flatten out and seem to converge to the k^{-3} slope (Fig. 3.9). Below the boundary layer the viscosity and isotropization effects are more relevant, leading to the geostrophic balance again. This can be perturbed by ageostrophic components of frontal circulation, mixed layer turbulence or Ekman flows (Callies and Ferrari, 2013).

This ageostrophic secondary circulation (ASC) associated to filaments and smaller eddies in the Guajira Peninsula and leeward of island. Note that this ASC are activated

in the more energetic zones of the basin, it could be the way as the smaller scales answer to the input or enhancing of EK in the scale closed to the deformation radius L_D. This means that the submesoscale inertial range attempts to counteract lightly the input of KE in the mesoscale. Whether the ASC's effect is larger, it could be enough as for modified the transference of KE in the upper ocean (Klein et al., 2008).

By computing the KE spectra from geostrophic and ageostrofic velocity decompositions, we can identify which terms control the KE transfer at different wavenumbers. (Fig. 3.10). The KE spectra for geostrofic (red dots), ageostrophic (blue dots) and total velocities (green line) from our solution, shows the dominance of the geostrophic decomposition at smaller wavenumbers in the three areas analysed. On both sides of the Lesser Antilles (center and right panels), the spectrum of geostrophic velocities matches with the spectrum of the total velocities, which shows the dominance of geostrophic terms over the whole spectral range. At high wavenumbers, the shallower slope of the KE spectrum of ageostrophic velocities on both sides of the Lesser Antilles demonstrate the potentially importance of the ageostrophic dynamics in these regions. In contrast, in the Colombia region the spectrum of the total velocities converges toward the spectrum of the ageostrophic velocities at higher wavenumbers ($k > 5 \times 10^{-4} [m^{-1}] \sim \lambda \approx 10 km$). This suggests that ageostrophic velocities induced by frontogenesis at smaller scales may contribute to the increase in EKE at larger scales in the Caribbean, as suggested by Jouanno et al. (2012).

3.3.3 KE spectral Decomposition

In order to understand the energetic impact of the each term of momentum balance, and how are transferred or dissipated the KE in the each scale, we compute a spectral decomposition multiplying the spectra of each term by the spectra of horizontal velocities following the same method as in Capet et al. (2008c). Prior to this analysis we remove the areal mean and apply a Hanning function on each term, which has the effect of
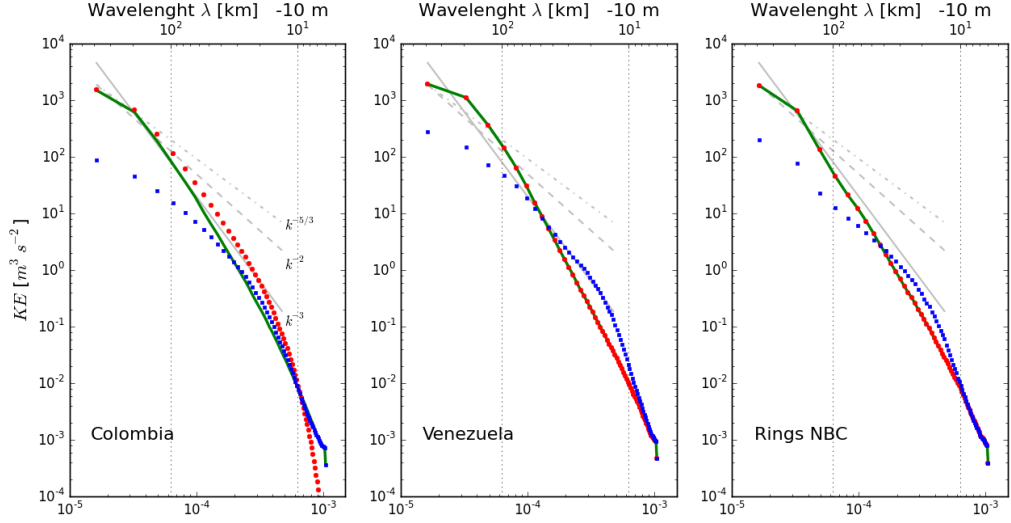
Figure 3.10: KE spectrums from geostrophic (red dots) and ageostrophic velocities(blue dots) and total velocity out from simulation (green line)

smoothing the advective horizontal fluxes through the boundaries. Therefore the sum of all terms results in the time tendency T denoted as

$$A(k) = A_h + A_v = \Re \left[-\widehat{u_h^*} \cdot \widehat{(u_h \cdot \nabla)u_h} - \widehat{u_h^*} \cdot \widehat{w \frac{\partial u_h}{\partial z}} \right] \tag{3.4}$$

where η and z_o represent the free surface elevation and the depth of the boundary layer (our case is $z_o = -50m$), respectively. In the second line from left to right, we have the dominant terms of the KE budget in the momentum equetions: the centered horizontal advection A_h, the vertical advection A_v, the pressure P, the horizontal Dissipation D_h and the vertical dissipation D_v. Pressure work P implicitly contains the local injection of KE from the conversion of potential to kinetic energy I. Each term was computed in function of the wavenumber (k) as follows:

$$P(k) = \Re \left[-\frac{1}{\rho_o} \widehat{u^*} \cdot \widehat{\nabla P} \right] \tag{3.5}$$

$$I(k) = \Re \left[\widehat{w^* \widehat{b}} \right] \tag{3.6}$$

$$D_h(k) = A_h^{up3} - A_h \tag{3.7}$$

$$D_v(k) = \Re \left[-\widehat{u_h^*} \cdot \frac{\widehat{\partial K_v \frac{\partial u_h}{\partial z}}}{\partial a} \right] \tag{3.8}$$

Here b is the buoyancy $(-g\rho/\rho_o)$ and K_v is the vertical viscosity. The overline represents a time average over the diagnostic interval which can vary depending on the time of interest. In our case we use a time interval of 2 months in order to assess how the KE budget varied on seasonal timescales. The caret denotes the horizontal FFT and the asterisk notation $*$ indicates the complex conjugate operator. The symbol $\Re$ is the operator that selects the real part of the spectral analysis. The horizontal dissipation is a function of the discretization used in ROMS, namely the upstream-biased scheme (Shchepetkin and McWilliams, 1998) and, as explained in Capet et al. (2008c) is defined as the difference between advection terms A_h^{up3} that are calculated by the third-order upwind scheme (Kowalik and Murty, 1993) and A_h that corresponds to the centered discretization schemes. Finally the vertical dissipative terms D_v represent the total contribution of energy dissipation, vertical diffusive flux in the boundary layer and the work done by the wind. The K_v usually varies in the vertical, being large in the boundary layer and practical vanished in the deeps. For our analysis we used the constant $K_v = 10^{-2}$ in the first 100 m depth.

This KE balance is sensitive to the wind stress variation, to the local restratification field, to the KPP parametrization used in the model and to the averaging time scale. We apply the KE budget decomposition to the same three where spectral analysis was performed (Colombia, Venezuela and Rings basin) in order to determine the dominant

terms in each region. We compute the KE budget for the season with the strongest winds (Dec-Jan), when the ITCZ is located in its southernmost position, and for season with moderate winds (May-Jun), when the ITCZ is in its northernmost position. We use the average of two months in the KE budget analysis to give continuity to the mesoscale processes, e.g. arrived of NBC rings or upwelled filament which appear at final of first month, assumed this time enough to represent each event.

The KE spectral balance is shown in the Figs. 3.11 and 3.12 for the strong and moderate wind seasons. We separated the KE balance in the mesoscale $k > 2 \times 10^{-5}[m^{-1}]$ (top) and submesoscale range $k > 2 \times 10^{-4}[m^{-1}]$ (middle). We can see the energetic contribution of each term of the momentum balance, noting that the KE injection I is more effective in the Colombia basin in summer, as a consequence of conversion from potential to kinetic energy via baroclinic instabilities in the regions (Jouanno et al., 2009). This input of energy is mostly counteracted by the vertical dissipation D_v on all wavenumbers, being larger than all other terms. This term depends of the KPP parametrization, the vertical diffusive flux in the upper ocean and of the synoptic wind forcing as suggested by Capet et al. (2008c). In the submesoscale range the advection terms A help to redistribute this injection of KE in the neighboring wavenumbers. The pressure P has a peak around $200km$ in the Colombian and Rings regions, a lenghtscale similar to the diameter of mesoscale eddies that are common in the region (Richardson (2005),(Fratantoni and Richardson, 2006)), with no relevant effects in the KE budget at submesoscale range. The horizontal dissipation D_h has fluctuations in the whole k range, maybe due to topographic effects in the circulation or the upstream discretization of advetive terms.

Potentially the advection terms A are not sources neither sinks of energy, instead they redistribute energy across different length scales (Scott and Wang, 2005). Positive and negative values of A show the direction in which KE is being transferred, depending of the mode (BC or BT) as the advection transfers the energy can be transferred forward

or inverse cascade direction. It results in a source or sink of KE for the neighbour scales. In the mesoscale range, A is negative over the Colombia and Rings areas, whereas in the Venezuela it is positive, this difference might be due to the dominance of BC (BT) mode circulation over the Colombia (Venezuela) basin (Jouanno et al., 2012). In the submesoscale range ($k > 4 \times 10^{-4}[m^{-1}] \sim \lambda < 15km$), A has some fluctuations close to zero over the two areas nearness to Antilles, which may be a consequence of the interaction of impinging eddies and currents on the topography. In general, A helps to counteract the effect of I in the balance of KE transference to smaller scales. Notice that this effect is negligible or opposite during the winter period, becoming a source of KE, which shows the seasonal variability of these processes in the studied areas.

In Fig. 3.12 we show the balance of KE transference for the period of weaker winds. The most notable differences are the weakening of I in the mesoscale range, followed by a change of sign of A terms in the Colombia and Rings basins in small wavenumbers. Addicionaly we note an increase of I and P in the submesoscale regime. Therefore, toward the submesoscale range (higher k) all terms are similarly important. Positive values of I are counteracted by A, D_v and D_h in the Colombia basin in the submesoscale regime, while in the two other zones the effect of A is less significant, enhancing the likelihood of transference of KE toward larger scales by advective processes as the flow advance to westward. Note that in the Rings area, D_v is higher than A and D_h, this explains how is I mainly compensated by dissipative effect, in direct EK cascade.

Figure 3.11: Spectral KE budget $[m^3.s^{-3}]$ in the mesoscale range (top) and submesoscale range (middle) for the Colombia basin (left column), Venezuela basin (middle column) and Streamward of island (rightcolumn) for the boreal summer of 2001 (Jun-Jul). The KE transfer function $\pi(k)$ $[m^2.s^{-3}]$ for each basin (bottom)
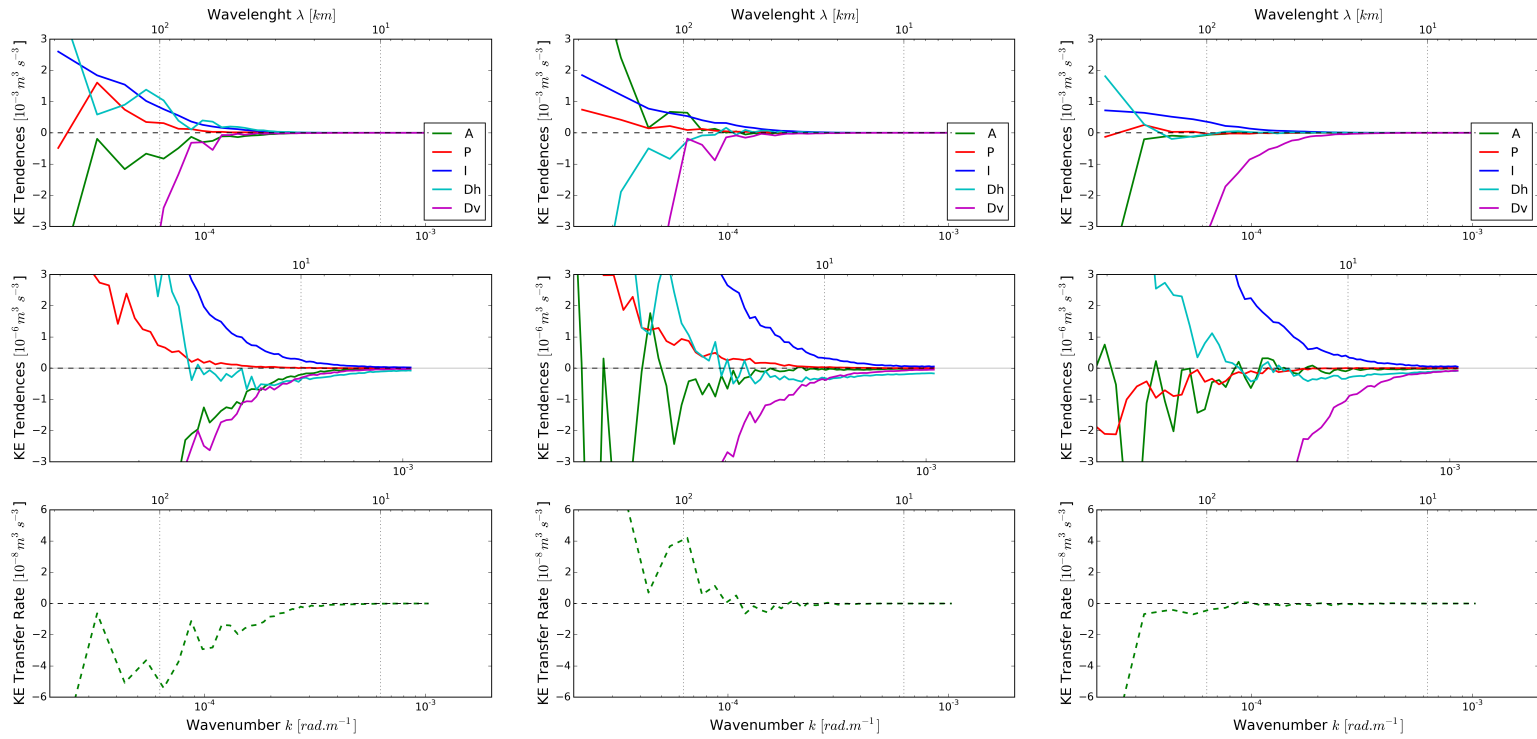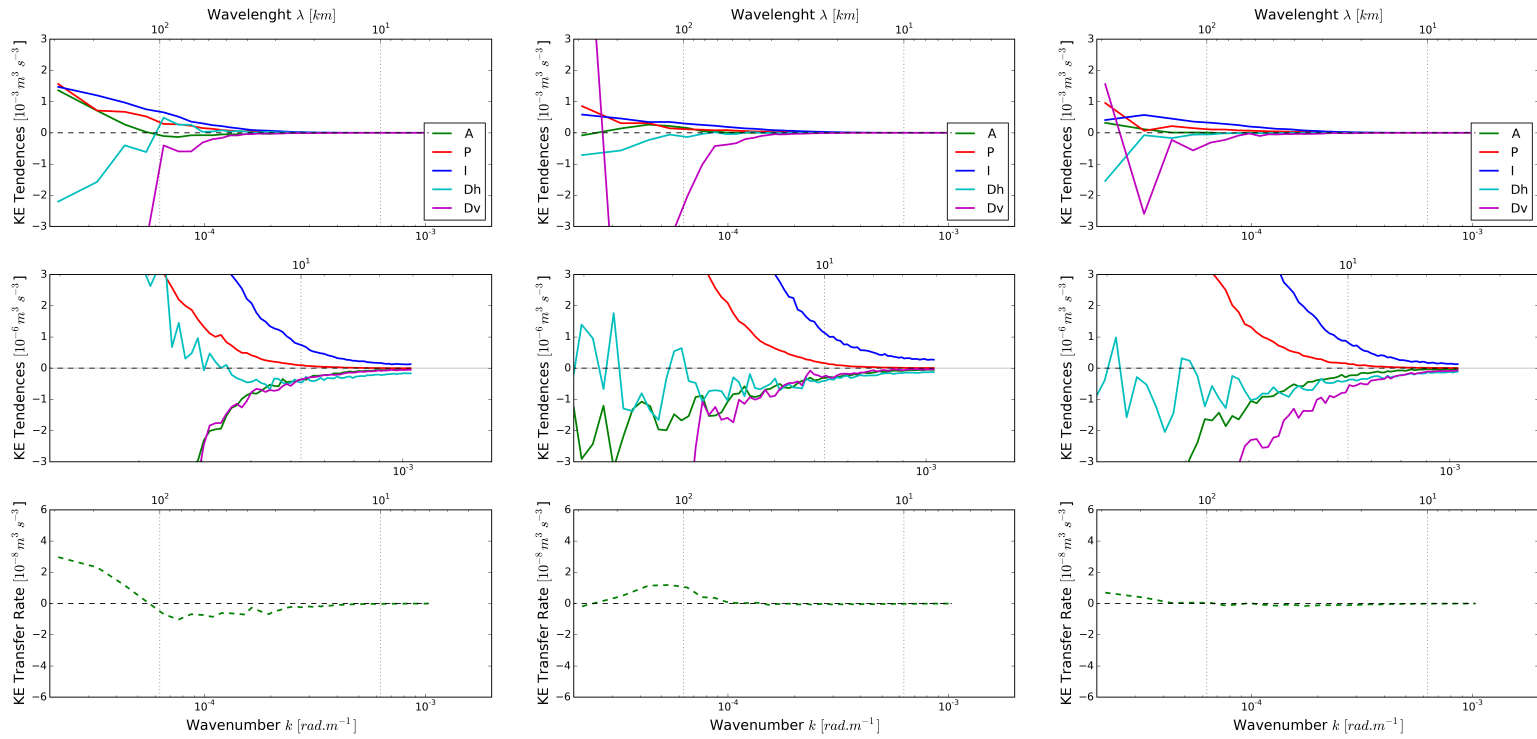
Figure 3.12: Spectral KE budget $[m^3.s^{-3}]$ in the mesoscale range (top) and submesoscale range (middle) for the Colombia basin (left column), Venezuela basin (middle column) and Streamward of island (rightcolumn) for the boreal winter of 2001 (Dec-Jan). The KE transfer function $\pi(k)$ $[m^2.s^{-3}]$ for each basin (bottom)

In Fig.3.2 we summarize the dominant balance in mesoscale and submesoscale regime for each season and each area, resulting in two main features: Firstly, the dissipative terms D_v dominate the momentum balance in the mesoscale regime. Such dominance is established through vertical diffusive processes and their parametrization on the boundary layer. Secondly, in the submesoscale regime the injection of KE, I, dominates over all other terms, except for the Rings area during moderate winds (May-Jun), where the dissipative effect dominates over the energetic injection at smaller scales. Note that term A can change sign (transferring upward or downward cascade) on the Colombia and Rings areas. Simultaneously the dissipative role of D_h changes of sign, depending directly to A and upstream discretization. It highlights the manner in which A interacts with D_v in the rings dissipative process, allowing the splitting of NBC rings in to smaller eddies that have peak.

Table 3.2: Spectral KE balance: This balance is doing above the KE tranferences in the Fig. 3.11 and Fig. 3.12, where it separate the mesoscale and submesoscale range at $k = 2 \times 10^{-4} \sim \lambda = 30km$. The first and second rows in each basin are for winter and summer season respectly.

Basin	Mesoscale Range		Submesoscale Range	
	$k > 2 \times 10^{-4}$		$k < 2 \times 10^{-4}$	
Colombia	$I + P + D_h$	$< D_v + A$	$I >$	$D_v + D_h + A$
	$I + P + A$	$< D_v + D_h$	$I >$	$D_v + D_h + A$
Venezuela	$I + P + A$	$< D_v + D_h$	$I >$	$D_v + D_h$
	$I + P + A$	$< D_v + D_h$	$I >$	$D_v + D_h + A$
Rings	$I + P + D_h$	$< D_v + A$	$I <$	$D_v + D_h$
	$I + P + A$	$\sim D_v + D_h$	$I >$	$D_v + D_h + A$

3.3.4 Spectral Energy Flux: KE Source and Sink

The slope $k^{-5/3}$ or k^{-3} between the spectral KE density and wavenumber k displays the pathway of energy and enstrophy cascade in 2-D turbulence, respectively, but as explains before, the $k^{-5/3}$ can vary from 2-D to 3-D turbulence theory. Hence, this spectra does not indicate the direction of the cascade, since the same result holds for

both the inverse cascade of 2-D turbulence and the direct cascade of 3-D turbulence. The spectral KE flux $\pi(k)$ is defined as the flux of energy (including the potential energy) through total wavenumber k range. Physically, this rate of transfer arises through the advective terms in the kinetic energy equation. Thus, it is based on the integration of term A of the KE balance (horizontal and vertical advection are includes) in all wavenumbers range. Assuming that the lateral flux is vanished through of previous application of the Hanning smoothing and the flux at the smallest scales (k_{max}) is vanished:

$$\pi(k) = \int_{k}^{k_{max}} A(k)dk \tag{3.9}$$

The bottom panel of Figs. 3.11 - 3.12 shows the KE rate of transfer of energy $\pi(k)$ in the k space. The KE flux $\pi(k)$ has various negative peaks in the mesoscale range of the Colombia region, suggesting an inverse KE cascade toward larger scales through the barotropization process descrived by Scott and Wang (2005), i.e. the conversion from the BC mode on smaller scalles to the BT mode in scales similar or larger to the deformation radius L_D. Thus, the positive slope of π continues until the submesoscale range at approximately $20km$, indicating a source of KE or inverse cascade to larger scales near these wavenumbers. For $k > 3 \times 10^{-4}[m^{-1}]$ the flux of energy is flattened close to zero assuming that the KE balance is reached by all terms on smallest scales and therefore there is no energy for transfer toward the smaller scales. In contrast, the Venezuela basin presents $\pi > 0$ in the mesoscale regime, with a peak around $100km$ that might be explained as source of KE by eddies with the same scale (Richardson, 2005). Upon reaching this scale π diminishes and crosses zero at $k = 1 \times 10^{-4}[m^{-1}]$, changing from downward to upward cascade flux in scales between $30 - 60km$ where it varies slightly and tends asymptotically to zero. From there on it has some wiggles, around $\pi \approx 0$ as resulting of dissipation process in small scales.

Lastly, on the Rings area the transference KE is null $\pi \approx 0$ across all scales possible due to the compensation among the injection and dissipation terms, presenting an inertial range between the $100 - 200km$. The considerable increase $\pi < 0$ in higher scales $(k < 3 \times 10^{-5}[m^{-1}] \sim \lambda > 200km)$ can be attributed to the advection of NBCr and their subsequent demised after impinging on the islands.

For the stronger wind season, the KE transfer rate shows positive values on the mesoscale over the Colombia basin, with a direct KE cascade $k < 6 \times 10^{-6}[m^{-1}] \sim \lambda \approx 100km$. Upon $\pi(k)$ inverts sign, transferring energy to larger scales than L_D and being consistent with the growth of eddy size suggested by (Jouanno et al., 2009). Then, it reaches a plateau in negative values between the 40-80 km, corresponding to Rossby deformation radius on the surrounding of Caribbean (Chelton et al., 1998). This range is defined as the inertial range because it is neither a source nor a sink of energy. At smaller scales we observe a smooth raising of slope emphasizing the idea that in the submesoscale range there is a direct KE cascade toward smaller scales k_{max}. Note in the middle-left panel of Fig.3.12 that I in the submesoscale regime is larger than the other terms in the Colombia region. In this cases, A works as a constant energy flux (excess energy of I on each scale) toward smaller scales, without the need to be a source or sink of energy. It contrast, the Venezuela region has a small source of KE in the mesoscale regime, that reaches its inertial range around to $100km$, from here it transfers all KE to smaller scales. While in all ranges of the Rings area the $\pi(k)$ is practically vanished, except in the larger scales $4 \times 10^{-5}[m^{-1}] \sim \lambda \approx 150km$ that can be attributed to the arrival of NBC rings.

Chapter 4

Summary and Conclusions

Although the Caribbean Sea is relatively homogeneous, this study shows that turbulent properties may vary not only temporally but also regionally, with consequences for the KE transfer rate in each of these regions. We analyse three regions with different turbulent features, namely, The east of the Lesser Antilles, where NBC rings impinge on the topography, the Venezuelan Region which includes the wake flow of the Antilles, and the Colombian region where coastal upwelling filaments interact with the mesoscale circulation.

Our results shows that frontogenesis associated with regions of high EKE in the Caribbean Sea, as such the lee of islands and the Guajira Upwelling (Fig. 3.7). On the latter, regions submesoscale processes, that result from the interaction between mesoscale currents and the upwelling filaments, act to re-stratify the mixed layer but this effect is hindered by the strong horizontal currents that counteract those effect by mixing the base of boundary layer (Fig. 3.6).

In tems of KE transference, at scales close to L_D, an inertial range is observed in terms of enstrophy ($90 \leq \lambda \leq 200km$) in the Colombian and Venezuelan regions, as can see in the flatten off of the compensate spectra (dotted lines of 3.8). We refer to enstrophy as the potential vorticity conservation along the whole wavenumber range,

thus, the increase of EKE inside of the Caribbean generates an inertial range that is absent to the east of the islands, where the KE is dissipated abruptly at scales closely to deformation radius, as can seen in the transfer rate of KE in Figs. 3.11 - 3.12.

Spectral analysis of ageostrophic velocities is consistent with previous state, showing the importance of these terms at smaller scales (Fig. 3.10), increasing the KE in the Venezuelan region and being dominant on the smaller scales in the Colombian Region.

The descomposition of the KE spectra, shows that any injection of energy in the mesoscale circulation is counteracted by the dissipative terms, while the advective terms transfer this energy for neighbouring spatial scales, either up or downward cascade. In the submesoscale range the injection of KE is higher in winter, when the winds are stronger, than the summer. The dissipative terms compensates all the KE injected in the summer, while in the winter, the advective terms distribute this KE input in a larger range of scales, having a significant contribution in favour of dissipative effects.

To complete our analysis, the transfer rate of each regions shows a different range of scales. In the east of Antilles there is a strong effect of dissipation in scales similar to that of NBC rings ($\lambda \approx 200\ km$), while in the submesoscale range, this transference rate is almost zero. Venezuelan region shows a peak at spatial scales close to L_D, which is attributed to the smaller eddies moving westward that can gain or loose KE. Whereas the submesoscale range of transfer rate has little wiggles around of zero, with forward KE cascade. In contrast, the Colombian region has the most variation of this transfer rate. In the strong wind season the KE at scales closed to L_D is transfered forward cascade, having an inertial range larger than in the other regions ($30km \leq \lambda \leq 80km$). In the moderated wind season, a KE inverse cascade can occur at larger scales than L_D, while smaller scales are transfered downward cascade and the inertial range only appears at smaller scales than $30\ km$.

This does not mean that this is the seasonal variability of each term in the KE budget, since that in our analysis we only take two representative seasons of two-years

of diagnostic period, based in the wind speed intensification and the arrive of the NCB ring in the Lesser Antilles and the main goal of our analysis is compare the meso- and submesoscale dynamics, from the energy perspective in three regions of the Caribbean Sea.

Despite the dominance of the dissipative terms over the mesoscale circulation in the Caribbean, (as shown in the KE budget Fig.s 3.11 - 3.12), we can see that on submesoscale ranges the injection terms are equal or higher than dissipative terms, which suggests that the conversion from potential to kinetic energy can dominate the balance in these scales during sporadic injection events. The transfer of energy up- or down cascade depends strongly on the diffusivity parametrization, which, in turn, depends on the model resolution and the discretization methods used in the filtering of the data. Increased model resolution allows a better representation of the smaller scale eddies that extract energy from the mesoscale thus increasing the forward cascade which will be dependent on the stratification of the mixed layer. Therefore regardless of the fact that some scales act as a source or sink of KE, the submesoscale will always induce the flow to its least energy state (i.e. towards KE zero and the lower PE possible).

The increase of KE observed in the Guajira Upwelling is due to the strong ageostrophic circulation within filaments and fronts, probably associated with surface frontogenesis, as seen in the high strain and shear rates (Shcherbina et al., 2013) shown in Fig. 3.4. This coincides with restratification induced by the heat flux divergence shown in Fig. 3.6. Thus, downward and upward vertical velocities due to surface frontogenesis could be and complementary explanation of the fluxes modelled by Jouanno and Sheinbaum (2013) in the same region. In particular the downward fluxes are substantially stronger when submesoscale processes are better resolved.

Bibliography

Andrade, C. A. and Barton, E. D. (2005). The guajira upwelling system. *Continental Shelf Research*, 25(9):1003–1022.

Athié, G., Candela, J., Ochoa, J., and Sheinbaum, J. (2012). Impact of caribbean cyclones on the detachment of loop current anticyclones. *Journal of Geophysical Research: Oceans*, 117(C3).

Bernal, G., Poveda, G., Roldán, P., and Andrade, C. (2006). Patrones de variabilidad de las temperaturas superficiales del mar en la costa caribe colombiana. *Rev. Acad. Colomb. Cienc*, 30(115):195–208.

Boccaletti, G., Ferrari, R., and Fox-Kemper, B. (2007). Mixed layer instabilities and restratification. *Journal of Physical Oceanography*, 37(9):2228–2250.

Callies, J. and Ferrari, R. (2013). Interpreting energy and tracer spectra of upper-ocean turbulence in the submesoscale range (1–200 km). *Journal of Physical Oceanography*, 43(10):2456–2474.

Capet, X., McWilliams, J., Molemaker, M., and Shchepetkin, A. (2008a). Mesoscale to submesoscale transition in the california current system. part ii: Frontal processes. *Journal of Physical Oceanography*, 38(1):44–64.

Capet, X., McWilliams, J. C., Molemaker, M. J., and Shchepetkin, A. (2008b). Mesoscale to submesoscale transition in the california current system. part i: Flow structure, eddy flux, and observational tests. *Journal of Physical Oceanography*, 38(1):29–43.

Capet, X., McWilliams, J. C., Molemaker, M. J., and Shchepetkin, A. (2008c). Mesoscale to submesoscale transition in the california current system. part iii: Energy balance and flux. *Journal of Physical Oceanography*, 38(10):2256–2269.

Casey, K. S., Brandon, T. B., Cornillon, P., and Evans, R. (2010). The past, present, and future of the avhrr pathfinder sst program. In *Oceanography from space*, pages 273–287. Springer.

Chelton, D. B., Deszoeke, R. A., Schlax, M. G., El Naggar, K., and Siwertz, N. (1998). Geographical variability of the first baroclinic rossby radius of deformation. *Journal of Physical Oceanography*, 28(3):433–460.

Cushman-Roisin, B. and Beckers, J.-M. (2011). *Introduction to geophysical fluid dynamics: physical and numerical aspects*, volume 101. Academic Press.

Fratantoni, D. M. and Richardson, P. L. (2006). The evolution and demise of north brazil current rings*. *Journal of physical oceanography*, 36(7):1241–1264.

Johns, W. E., Townsend, T. L., Fratantoni, D. M., and Wilson, W. D. (2002). On the atlantic inflow to the caribbean sea. *Deep Sea Research Part I: Oceanographic Research Papers*, 49(2):211–243.

Jouanno, J. and Sheinbaum, J. (2013). Heat balance and eddies in the caribbean upwelling system. *Journal of Physical Oceanography*, 43(5):1004–1014.

Jouanno, J., Sheinbaum, J., Barnier, B., and Molines, J.-M. (2009). The mesoscale

variability in the caribbean sea. part ii: Energy sources. *Ocean Modelling*, 26(3):226–239.

Jouanno, J., Sheinbaum, J., Barnier, B., Molines, J. M., and Candela, J. (2012). Seasonal and interannual modulation of the eddy kinetic energy in the caribbean sea. *Journal of Physical Oceanography*, 42(11):2041–2055.

Jouanno, J., Sheinbaum, J., Barnier, B., Molines, J.-M., Debreu, L., and Lemarié, F. (2008). The mesoscale variability in the caribbean sea. part i: Simulations and characteristics with an embedded model. *Ocean Modelling*, 23(3):82–101.

Klein, P., Hua, B. L., Lapeyre, G., Capet, X., Le Gentil, S., and Sasaki, H. (2008). Upper ocean turbulence from high-resolution 3d simulations. *Journal of Physical Oceanography*, 38(8):1748–1763.

Kowalik, Z. and Murty, T. S. (1993). Numerical modeling of ocean dynamics.

Marchesiello, P., Capet, X., Menkes, C., and Kennan, S. C. (2011). Submesoscale dynamics in tropical instability waves. *Ocean Modelling*, 39(1):31–46.

Murphy, S. J., Hurlburt, H. E., and O'Brien, J. J. (1999). The connectivity of eddy variability in the caribbean sea, the gulf of mexico, and the atlantic ocean. *Journal of Geophysical Research: Oceans*, 104(C1):1431–1453.

Oey, L.-Y., Lee, H.-C., and Schmitz, W. J. (2003). Effects of winds and caribbean eddies on the frequency of loop current eddy shedding: A numerical model study. *Journal of Geophysical Research: Oceans*, 108(C10).

Penven, P., Echevin, V., Pasapera, J., Colas, F., and Tam, J. (2005). Average circulation, seasonal cycle, and mesoscale dynamics of the peru current system: A modeling approach. *Journal of Geophysical Research: Oceans*, 110(C10).

Qiu, B., Chen, S., Klein, P., Sasaki, H., and Sasai, Y. (2014). Seasonal mesoscale and submesoscale eddy variability along the north pacific subtropical countercurrent. *Journal of Physical Oceanography*, 44(12):3079–3098.

Richardson, P. (2005). Caribbean current and eddies as observed by surface drifters. *Deep Sea Research Part II: Topical Studies in Oceanography*, 52(3):429–463.

Rueda-Roa, D. T. and Muller-Karger, F. E. (2013). The southern caribbean upwelling system: Sea surface temperature, wind forcing and chlorophyll concentration patterns. *Deep Sea Research Part I: Oceanographic Research Papers*, 78:102–114.

Scott, R. B. and Wang, F. (2005). Direct evidence of an oceanic inverse kinetic energy cascade from satellite altimetry. *Journal of Physical Oceanography*, 35(9):1650–1666.

Shchepetkin, A. F. and McWilliams, J. C. (1998). Quasi-monotone advection schemes based on explicit locally adaptive dissipation. *Monthly Weather Review*, 126(6):1541–1580.

Shchepetkin, A. F. and McWilliams, J. C. (2005). The regional oceanic modeling system (roms): a split-explicit, free-surface, topography-following-coordinate oceanic model. *Ocean Modelling*, 9(4):347–404.

Shcherbina, A. Y., D'Asaro, E. A., Lee, C. M., Klymak, J. M., Molemaker, M. J., and McWilliams, J. C. (2013). Statistics of vertical vorticity, divergence, and strain in a developed submesoscale turbulence field. *Geophysical Research Letters*, 40(17):4706–4711.

Simmons, H. L. and Nof, D. (2002). The squeezing of eddies through gaps. *Journal of physical oceanography*, 32(1):314–335.

Thomas, L. N., Tandon, A., and Mahadevan, A. (2008). Submesoscale processes

and dynamics. *Ocean Modeling in an Eddying Regime, Geophys. Monogr. Ser*, 177:17–38.

Vallis, G. (2006). Atmospheric and oceanic fluid dynamics: Fundamentals and large-scale circulation (cambridge).

Wang, C., Enfield, D. B., Lee, S.-k., and Landsea, C. W. (2006). Influences of the atlantic warm pool on western hemisphere summer rainfall and atlantic hurricanes. *Journal of Climate*, 19(12):3011–3028.
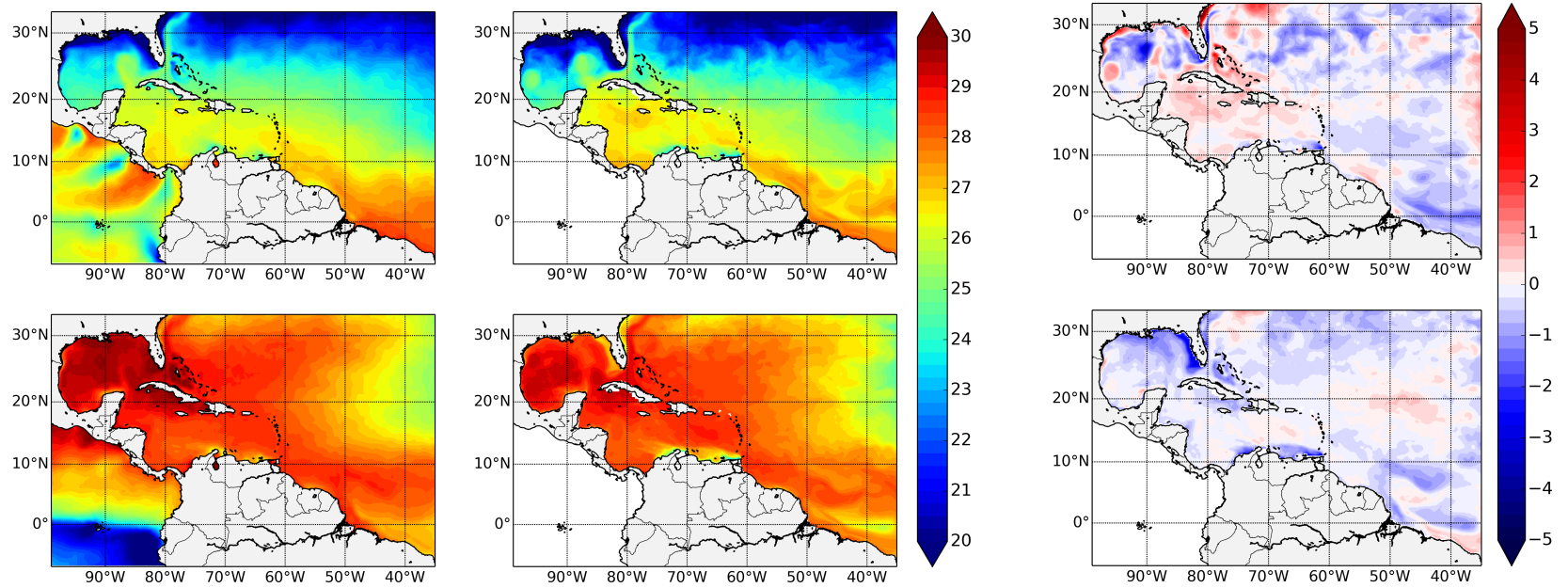
Figure 1: Seasonal Sea Surface Temperature (SST) in boreal winter (upper panels) and summer (lower panels) from AVHRR satellite observation (left column), simulation (center column) and the difference (right column) between them
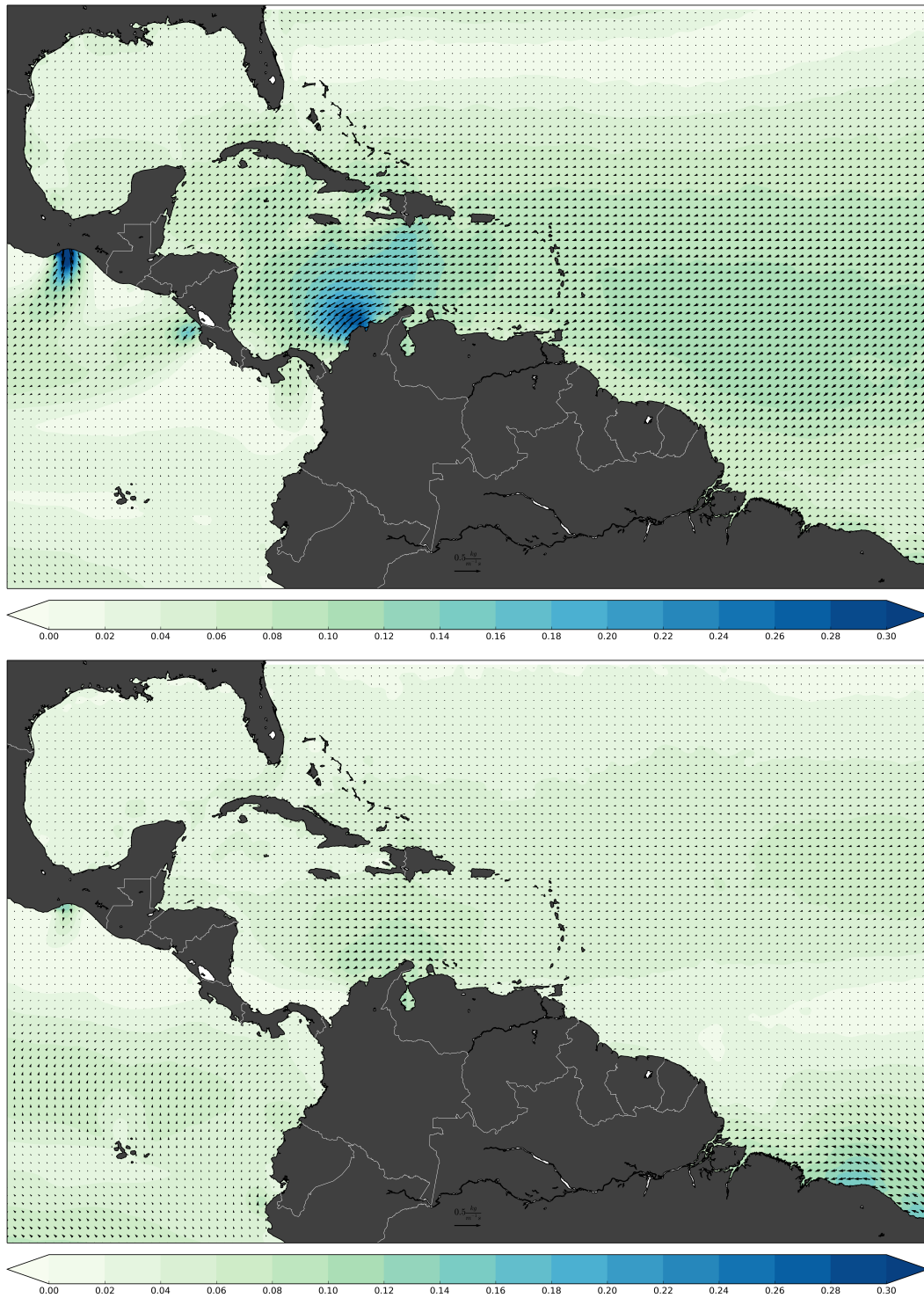
Figure 2: Seasonal wind stress for the boreal winter (top) and for the boreal summer (bottom) when the ITCZ is located over the continent and over the Caribbean basin respectively. Unities in $kgm^{-1}s^{-1}$